DMD Fast Forward. Published on March 7, 2007 as DOI: 10.1124/dmd.106.013649
DMD Fast Forward. Published on March 7, 2007 as doi:10.1124/dmd.106.013649
This article has not been copyedited and formatted. The final version may differ from this version.

GENOTOXICITY OF 2-(3-CHLOROBENZYLOXY)-6-(PIPERAZINYL)PYRAZINE, A NOVEL 5-HT2C RECEPTOR AGONIST FOR THE TREATMENT OF OBESITY: ROLE OF METABOLIC ACTIVATION

Amit S. Kalgutkar*, Deepak K. Dalvie, Jiri Aubrecht, Evan B. Smith, Stephanie L. Coffing, Jennifer R. Cheung, Chandra Vage, Mary E. Lame, Phoebe Chiang, Kim F. McClure, Tristan S. Maurer, Richard V. Coelho Jr., Victor F. Soliman, Klaas Schildknegt

Pharmacokinetics, Dynamics and Metabolism, Pfizer Global Research and Development, Groton, Connecticut (A.S.K., C.V., M.E.L., T.S.M., V.F.S.) and La Jolla, California (D.K.D., E.B.S.); Safety Sciences (J.A., S.L.C., J.R.C.); Cardiovascular and Metabolic Diseases Chemistry (P.C., K.F.M.); and Chemical Research and Development (K.S.), Pfizer Global Research and Development, Groton, Connecticut

Downloaded from dmd.aspetjournals.org at ASPET Journals on May 23, 2024

Copyright 2007 by the American Society for Pharmacology and Experimental Therapeutics.

DMD Fast Forward. Published on March 7, 2007 as DOI: 10.1124/dmd.106.013649
This article has not been copyedited and formatted. The final version may differ from this version.

Running Title: Bioactivation of a piperazine analog to genotoxic metabolites

Number of Text Pages: (including references) 28

Number of Tables: 2

Number of Figures: 12

Number of References: 26

Number of Words in Abstract: 251

Number of Words in Introduction: 527

Number of Words in Discussion: 1105

Abbreviations used are: 5-HT, 5-hydroxytryptamine; **3**, 2-(3-chlorobenzyloxy)-6-(piperazin-1-yl)pyrazine; **5**, 6-(3-chlorobenzyloxy)-N-(2-aminoethyl)pyrazin-2-amine; **1**, *tert*-butyl-4-(6-chloropyrazin-2-yl)piperazine-1-carboxylate; **2**, *tert*-butyl-4-(6-(3-chlorobenzyloxy)pyrazin-2-yl)piperazine-1-carboxylate; **4**, 2-(3-chlorobenzyloxy)-6-chloropyrazine; DMSO, dimethylsulfoxide; DPM, disintegrations per minute; LC-MS/MS, liquid chromatography tandem mass spectrometry; CID, collision-induced dissociation; MRM, multiple reaction monitoring; R_t, retention time.

Correspondence should be addressed to: Amit S. Kalgutkar, Pharmacokinetics, Dynamics, and Metabolism Department, Pfizer Global Research and Development, Groton, CT 06340. Phone: (860)-715-2433. E-mail: amit.kalgutkar@pfizer.com

Downloaded from dmd.aspetjournals.org at ASPET Journals on May 23, 2024

DMD Fast Forward. Published on March 7, 2007 as DOI: 10.1124/dmd.106.013649
This article has not been copyedited and formatted. The final version may differ from this version.

Abstract

2-(3-Chlorobenzyloxy)-6-(piperazin-1-yl)pyrazine (**3**) is a potent and selective 5-HT_{2C} agonist that exhibits dose-dependent inhibition of food intake and reduction in body weight in rats making it an attractive candidate for treatment of obesity. However, examination of the genotoxicity potential of **3** in the *Salmonella* Ames assay using tester strains TA98, TA100, TA1535 and TA1537 revealed a metabolism (rat S-9/NADPH)- and dose-dependent increase of reverse mutations in strains TA100 and TA1537. The increase in reverse mutations was attenuated upon co-incubation with methoxylamine and glutathione. The irreversible and concentration-dependent incorporation of radioactivity in calf thymus DNA following incubations with [^{14}C]-**3** in the presence of rat S-9/NADPH suggested that **3** was bioactivated to a reactive intermediate that covalently bound DNA. In vitro metabolism studies on **3** with rat S-9/NADPH in the presence of methoxylamine and cyanide led to the detection of amine and cyano conjugates of **3**. The mass spectrum of the amine conjugate was consistent with condensation of amine with an aldehyde metabolite derived from hydroxylation of the secondary piperazine nitrogen-α-carbon bond. The mass spectrum of the cyano conjugate suggested a bioactivation pathway involving N-hydroxylation of the secondary piperazine nitrogen followed by two-electron oxidation to generate an electrophilic nitrone, which reacted with cyanide. The 3-chlorobenzyl motif in **3** was also bioactivated via initial aromatic ring hydroxylation followed by elimination to a quinone-methide species that reacted with glutathione or with the secondary piperazine ring nitrogen in **3** and its mono-hydroxylated metabolite(s). The metabolism studies described herein provide a mechanistic basis for the mutagenicity of **3**.

Downloaded from dmd.aspetjournals.org at ASPET Journals on May 23, 2024

DMD Fast Forward. Published on March 7, 2007 as DOI: 10.1124/dmd.106.013649
This article has not been copyedited and formatted. The final version may differ from this version.

Introduction

Advances in molecular biology and pharmacology have led to the identification of fourteen 5-hydroxytryptamine (serotonin, 5-HT) receptor subtypes (Hoyer et al., 2002). These subtypes are classified into seven receptor families (5-HT_1 to 5-HT_7) according to their structure, function, and signal transduction properties and are distributed widely in the central and peripheral nervous system. The 5-HT_2 receptor subfamily comprises three subtypes namely 5-HT_{2A}, 5-HT_{2B}, and 5-HT_{2C}. These receptors exhibit 46 to 50% sequence homology and belong to the large family of seven transmembrane domain G protein-coupled receptors. Each of these receptor subtypes has been implicated in the control of food intake. In particular, the 5-HT_{2C} receptor has been the focus of many studies investigating feeding behavior. Evidence from transgenic mice with a targeted deletion of the 5-HT_{2C} receptor (Tecott et al., 1995) and pharmacological studies using specific 5-HT_{2C} receptor ligands (Bickerdike, 2003) supports a potential therapeutic utility of 5-HT_{2C} receptor agonists as anti-obesity agents. For instance, 5-HT_{2C} receptor deficient mice are obese, hyperphagic and exhibit impaired satiety. They also display elevated insulin and leptin levels and impaired glucose utilization (Tecott et al., 1995; Heisler et al., 1998; Nonogaki et al., 1998). Consistent with these observations, 5-HT_{2C} agonists have been reported to reduce food intake and body weight in animal models (Bickerdike, 2003; Kimura et al., 2004; Vickers and Dourish, 2004; Dunlop et al., 2005). Conversely, 5-HT_{2C} antagonists such as anti-psychotics increase food intake in rodents and cause weight gain in humans (Masand, 2000; von Meyenburg et al., 2003).

In the course of our efforts to identify novel 5-HT_{2C} receptor agonists, we discovered a new class of selective 5-HT_{2C} agonists as exemplified with 2-(3-chlorobenzyloxy)-6-

Downloaded from dmd.aspetjournals.org at ASPET Journals on May 23, 2024

DMD Fast Forward. Published on March 7, 2007 as DOI: 10.1124/dmd.106.013649
This article has not been copyedited and formatted. The final version may differ from this version.

(piperazin-1-yl)pyrazine (**3**) (Figure 1). **3** is a potent $5HT_{2C}$ receptor agonist, which displays functional selectivity for the $5HT_{2C}$ receptor over the other $5HT_2$ receptor subtypes. While **3** binds to human $5HT_{2C}$, $5HT_{2A}$ and $5HT_{2B}$ receptors subtypes with K_i values of 1.0, 8.4 and 34.0 nM, respectively, functional agonist activity (EC_{50} of 54 nM and 90% of maximal 5-HT activation) is observed only at the $5HT_{2C}$ receptor. In acute in vivo studies, oral administration of **3** to Wistar rats resulted in the dose-dependent inhibition of both spontaneous, nocturnal food intake and fasting-induced re-feeding. Furthermore, oral administration of **3** at 30 mg/kg daily to Wistar rats for four days resulted in ~ 8% inhibition of cumulative food intake and ~ 24% reduction in body weight over the four-day period. Unfortunately, **3** displayed a serious genetic safety liability that manifested as a positive finding in the *Salmonella* reverse mutation assay in presence of metabolic activation. The *Salmonella* assay has become an integral part of safety evaluation of drug candidates and is required by regulatory agencies for drug approvals worldwide. Since positive findings in the *Salmonella* reverse mutation assay have a good correlation with the outcome of rodent carcinogenicity testing, a positive result leads to the discontinuation of development particularly for drugs intended for non-life threatening indications (Kim and Margolin, 1999; Zeiger, 1998). To design follow-on $5\text{-}HT_{2C}$ agonists devoid of this issue, we set out to investigate the mutagenic mechanisms that led to a positive response in the *Salmonella* assay with **3**. The results of these studies are described herein.

Experimental Procedures

Chemicals. All chemicals and solvents used in chemical synthesis were purchased from the Aldrich Chemical Co. (Milwaukee, WI). The purity of products

Downloaded from dmd.aspetjournals.org at ASPET Journals on May 23, 2024

DMD Fast Forward. Published on March 7, 2007 as DOI: 10.1124/dmd.106.013649
This article has not been copyedited and formatted. The final version may differ from this version.

was judged to be at least 99% on the basis of their chromatographic homogeneity. ^{1}H NMR spectra in $CDCl_3$ or CD_3OD were recorded on a Varian Unity M-400 MHz spectrometer (Varian, Inc., Palo Alto, CA); chemical shifts are expressed in parts per million (ppm, δ) calibrated to the deuterium lock signal for $CDCl_3$ and CD_3OD. Spin multiplicities are given as s (singlet), d (doublet) and m (multiplet). NADPH, methoxylamine, glutathione and potassium cyanide were purchased from Sigma-Aldrich (St. Louis, MO). Aroclor 1254-induced Sprague-Dawley rat liver S-9 mixture was purchased from Molecular Toxicology (Boone, NC). The synthesis of 2-(3-chlorobenzyloxy)-6-(piperazin-1-yl)pyrazine (**3**) and 6-(3-chlorobenzyloxy)-N-(2-aminoethyl)pyrazin-2-amine (**5**), the major metabolite of **3** in rat S-9 fractions is shown in Figure 1.

Preparation of 2-(3-Chlorobenzyloxy)-6-(piperazin-1-yl)pyrazine (3). *Step I. tert-Butyl-4-(6-chloropyrazin-2-yl)piperazine-1-carboxylate* (**1**). A mixture of 2,6-dichloropyrazine (2.98 g, 20 mmol), piperazine-1-carboxylic acid-*tert*-butyl ester (3.72 g, 20 mmol) and sodium carbonate (2.12 g, 20 mmol) in *tert*-butanol (50 ml) was heated under nitrogen for 65 h. The solution was concentrated *in vacuo*. The residue was partitioned between ethyl acetate (50 ml) and water (50 ml). The aqueous phase was extracted with ethyl acetate (3 x 30 ml). The combined organic extracts were washed with brine (50 ml), dried over magnesium sulfate, filtered, and concentrated *in vacuo* to give **1** as a white solid. ^{1}H NMR ($CDCl_3$) δ 7.96 (s, 1H), 7.82 (s, 1H), 3.52-3.60 (m, 8H), 1.46 (s, 9H). MS (ES^+) Calc: 298.1, Found: 299.1 (M+1). *Step II. tert-Butyl-4-(6-(3-chlorobenzyloxy)pyrazin-2-yl)piperazine-1-carboxylate* (**2**). A mixture of **1** (300 mg, 1.0 mmol), 3-chlorobenzyl alcohol (0.142

Downloaded from dmd.aspetjournals.org at ASPET Journals on May 23, 2024

DMD Fast Forward. Published on March 7, 2007 as DOI: 10.1124/dmd.106.013649
This article has not been copyedited and formatted. The final version may differ from this version.

ml, 1.2 mmol), potassium hydroxide (191 mg, 3.4 mmol) and 18-crown-6 (10.6 mg, 0.04 mmol) in toluene (6 ml) was stirred under reflux for 5.5 h and concentrated *in vacuo*. The residue was partitioned between water (30 ml) and dichloromethane (30 ml). The aqueous phase was separated and extracted with dichloromethane (2 x 30 ml). The combined organic extracts were dried over magnesium sulfate, filtered, and concentrated *in vacuo*. The crude product was purified by preparative thin layer chromatography (5% methanol in dichloromethane) to afford 380 mg of **2**. ^{1}H NMR ($CDCl_3$) δ 7.63 (s, 1H), 7.59 (s, 1H), 7.40 (s, 1H), 7.27 (s, 3H), 5.26 (s, 2H), 3.51 (s, 8H), 1.46 (s, 9H). MS (ES^+) Calc: 404.1, Found: 405.0 (M+1). *Step III. Fumarate Salt of **3***. To a solution of **2** (380 mg, 0.94 mmol) in dichloromethane (6 ml) was added trifluoroacetic acid (1.4 ml). After stirring at room temperature for 2 h, the solution was concentrated *in vacuo*. The residue was partitioned between 1M HCl (20 ml) and ethyl acetate (30 ml). The aqueous phase was washed with ethyl acetate (2 x 30 ml), basified with 3 N NaOH, and extracted with ethyl acetate (3 x 30 ml). The combined organic extracts were concentrated *in vacuo* to afford the free base of **3** (252 mg) as an oil. ^{1}H NMR ($CDCl_3$) δ 7.62 (s, 1H), 7.56 (s, 1H), 7.40 (s, 1H), 7.28-7.25 (m, 3H), 5.26 (s, 2H), 3.49 (t, 4H), 2.95 (t, 4H), 1.96 (s, 1H). To a solution of the free base form of **3** (252 mg, 0.83 mmol) in a mixture of isopropyl ether (8 ml) and methanol (1 ml) was added 0.5 M fumaric acid in methanol (1.86 ml, 0.93 mmol) in a single portion. The resulting mixture was stirred at room temperature for 1 h. The white solid was collected by filtration and washed with isopropyl ether followed by hexane and dried *in vacuo* to afford the fumarate salt of **3**. ^{1}H NMR (CD_3OD) δ 7.77 (s, 1H),

Downloaded from dmd.aspetjournals.org at ASPET Journals on May 23, 2024

DMD Fast Forward. Published on March 7, 2007 as DOI: 10.1124/dmd.106.013649
This article has not been copyedited and formatted. The final version may differ from this version.

7.59 (s, 1H), 7.44 (d, 1H), 7.34-7.28 (m, 3H), 6.67 (s, 2H), 5.35 (s, 2H), 3.82-3.79 (m, 4H), 3.29-3.24 (m, 4H). MS (ES^+) Calc: 304.1, Found: 305.4 (M+1).

Synthesis of 6-(3-Chlorobenzyloxy)-N-(2-aminoethyl)pyrazin-2-amine (5), the Major Metabolite of 3 in Aroclor 1254-Induced Rat Liver S-9 Protein. *Step I. 2-(3-Chlorobenzyloxy)-6-Chloropyrazine* (**4**). To a solution of 3-chlorobenzyl alcohol (0.16 µl, 1.4 mmol) in tetrahydrofuran (5 ml) was added sodium hydride (60% in mineral oil, 67.2 mg, 1.68 mmol). After stirring at room temperature for 30 min, 2,6-dichloropyrazine (200 mg, 1.34 mmol) was added in one portion. The resulting mixture was refluxed for 1.5 h, cooled to room temperature and poured into water (50 ml). The aqueous solution was extracted with ethyl acetate (2 x 30 ml). The combined organic extracts were washed with brine, dried under magnesium sulfate, filtered, and concentrated. The residue was purified by preparative TLC (30% ethyl acetate in hexanes) to give **4** (328 mg).^{1}H NMR ($CDCl_3$) δ 8.18 (2s, 2H), 7.44 (s, 1H), 7.31 (2s, 3H), 5.34 (s, 2H). MS (ES^+) Calc: 254.0, Found: 255.2 (M+1). *Step II.* A mixture of **4** (290 mg, 1.1 mmol) and ethylene diamine (1.14 ml, 17.1 mmol) in dioxane (4 ml) was refluxed for 15 h. The solution was cooled to room temperature and poured into ice water (30 ml), extracted with ethyl acetate (3 x 20 ml). The combined organic extracts were extracted with 1N HCl and the aqueous solution was basified with 1N NaOH, extracted with ethyl acetate (3 x 30 ml). The combined organic extracts were washed with brine, dried under magnesium sulfate, filtered, and concentrated *in vacuo* to give **5** (258 mg). ^{1}H NMR ($CDCl_3$) δ 7.48 (s, 1H), 7.44 (s, 1H), 7.39 (s, 1H), 7.25 (m, 3H), 5.24 (s, 2H), 5.12 (m, 1H), 3.32-3.37 (m, 2H), 2.89 (m, 2H), 1.81 (broad s, 2H). MS (ES^+) Calc: 278.1, Found: 279.3 (M+1).

Downloaded from dmd.aspetjournals.org at ASPET Journals on May 23, 2024

DMD Fast Forward. Published on March 7, 2007 as DOI: 10.1124/dmd.106.013649
This article has not been copyedited and formatted. The final version may differ from this version.

Synthesis of [^{14}C]-2-(3-Chlorobenzyloxy)-6-(piperazin-1-yl)pyrazine ([^{14}C]-3).

*Step I. Preparation of [^{14}C]-2-(3-chlorobenzyloxy)-6-chloropyrazine ([^{14}C]-**4**).* Sodium *tert*-butoxide (42 mg, 0.44 mmol) was added to a solution of 3-chlorobenzyl alcohol (52 μl, 0.44 mmol) in 3 ml of tetrahydrofuran. A 1.5 ml portion of this solution was added dropwise to 2,6-dichloro-[2,3-^{14}C]pyrazine (7.75 mCi, 55 mCi/mmol, 0.14 mmol) (ChemSyn Laboratories, Lenexa, KS) over 2.5 h and the resulting solution was stirred at room temperature overnight. The reaction was then concentrated in *vacuo* and the resulting residue was purified by silica gel flash column chromatography, eluting with 5% acetone in hexane, to afford 4.56 mCi of [^{14}C]-**4**. *Step II.* Piperazine (48 mg, 0.56 mmol) was added to a solution of [^{14}C]-**4** (4.56 mCi, 55 mCi/mmol, 0.08 mmol) in 1 ml of water. The resulting suspension was heated at 90 °C for 32 h. The reaction was then cooled to room temperature, diluted with 5 ml of water and extracted twice with 5 ml portions of ethyl acetate. The combined ethyl acetate extracts were concentrated in *vacuo* and the resulting residue was purified by silica gel flash column chromatography, eluting with 10% methanol in dichloromethane, to afford 1.94 mCi of [^{14}C]-**3**.

Genetic Toxicity Studies. The *Salmonella* reverse mutation assay was performed using *Salmonella* typhimurium tester strains TA98, TA100, TA1535 and TA1537 (Maron and Ames, 1984). Briefly, the *Salmonella* cells were treated in soft agar overlays with **3** dissolved in dimethyl sulfoxide (DMSO) at concentrations ranging from 0.015 to 5 mg/plate or an appropriate amount of DMSO in presence or absence of aroclor 1254-induced rat liver S9 mixture and a NADPH-regenerating system. Incubations comprising of tester strain TA100, **3** (0.5 mg/plate), methoxylamine (1 mM) or glutathione (1 mM) in the presence or absence of aroclor 1254-induced rat liver S9 mixture and NADPH were

Downloaded from dmd.aspetjournals.org at ASPET Journals on May 23, 2024

DMD Fast Forward. Published on March 7, 2007 as DOI: 10.1124/dmd.106.013649
This article has not been copyedited and formatted. The final version may differ from this version.

also conducted to assess the effect of exogenously added nucelophiles on the mutagenic response of **3**. The number of visible revertant colonies present after 72 h incubation at 37°C was recorded and fold of change over DMSO-treated control plates was calculated. At least three independent experiments with each *Salmonella* tester strain were performed. The analysis of the data included calculating average and SEM. The statistical significance was determined using the t-test. A 2-fold statistically significant ($p \leq 0.05$) increase of number of revertant colonies over the DMSO-treated controls was considered as a positive response in the *Salmonella* assay.

In vitro Covalent Binding of [^{14}C]-3 to DNA. To emulate conditions of the *Salmonella* assay, calf thymus DNA (Sigma-Aldrich, St Louis, MO) was incubated with appropriate concentrations of [^{14}C]-**3** (specific activity 55 mCi/mmol) in the bacterial growth medium (Oxiod Nutrient Broth #2, BD, Franklin Lakes, NJ) in presence or absence of metabolic activation for 3 h at 37 °C. In the first set of experiments, metabolic activation was performed utilizing NADPH as cofactor. Incubations (volume = 1 ml) consisted of calf thymus DNA (1.0 mg/ml), **3** (0.5 μM), and 20 μl of aroclor 1254-induced rat liver S9 protein that was prepared separately by combining 0.5 ml S9 (protein concentration 38.4 mg/ml), 1.25 ml phosphate buffer and 36.5 mg NADPH. In the second set of experiments, a NADPH self-regenerating system was utilized instead of NADPH. Incubations (volume = 1 ml) comprised of calf thymus DNA (1.0 mg/ml), **3** (0.5 and 5 μM), and 139 μl S9 protein. The mixture was prepared by combining 100 μl S9 protein (protein concentration = 38.4 mg/ml), NADP monosodium (4 mM), glucose-6-phosphate (5 mM), potassium chloride (33 mM) and magnesium chloride (8 mM) in 900 μl of 100 mM sodium phosphate buffer (pH 7.4). All incubations in both test conditions were

Downloaded from dmd.aspetjournals.org at ASPET Journals on May 23, 2024

DMD Fast Forward. Published on March 7, 2007 as DOI: 10.1124/dmd.106.013649
This article has not been copyedited and formatted. The final version may differ from this version.

conducted in duplicate or triplicate and experiments included positive ([^{14}C]-benzo[a]pyrene (100 μM)) and vehicle (0.5% DMSO) controls. In addition, incubations were also conducted in the presence or absence of S9 protein. Incubations lacking NADPH co-factor were also included to test cytochrome P450-independent mechanisms of DNA binding by [^{14}C]-**3**. After incubation, unbound [^{14}C]-**3** was removed via extraction of the calf thymus DNA with phenol:chloroform:isoamyl alcohol (25:24:1) followed by two additional extractions with chloroform:isoamyl alcohol (24:1). The DNA was precipitated by the addition of 1/10 volume of 2 M NaCl and 2X volume of ethanol. After centrifugation (2000 x *g* for 10 min), the resulting DNA pellet was washed twice with ethanol, dissolved in 1x Tris-EDTA and quantified by ultraviolet spectroscopy (λ = 260 nm). Remaining DNA-bound radioactivity was measured on a Beckman LS6000IC liquid scintillation counter (Beckman Coulter). The results are expressed as mean counts (disintegrations per minute (DPM)) per 20 μg calf DNA.

Metabolism Studies. Stock solutions of the test compounds were prepared in methanol. The final concentration of methanol in the incubation media was 0.2% (v/v). Incubations were carried out at 37 ^{0}C for 60 min in a shaking water bath. The incubation volume was 1 ml and consisted of the following: 0.1 M potassium phosphate buffer (pH 7.4) containing $MgCl_2$ (10 mM), Aroclor 1254-induced rat liver S-9 fraction (final protein concentration = 1 mg/ml), NADPH (1 mM), substrate (20 μM), and methoxylamine (1 mM) or potassium cyanide (1 mM) or glutathione (1 mM). Incubations that lacked either NADPH or trapping agents served as negative controls, and reactions were terminated by the addition of ice-cold acetonitrile (1 ml). The solutions were centrifuged (3,000 x *g*, 15 min) and the supernatants were dried under a steady nitrogen

Downloaded from dmd.aspetjournals.org at ASPET Journals on May 23, 2024

DMD Fast Forward. Published on March 7, 2007 as DOI: 10.1124/dmd.106.013649
This article has not been copyedited and formatted. The final version may differ from this version.

stream. The residue was reconstituted with mobile phase and analyzed for metabolite formation by liquid chromatography tandem mass spectrometry (LC-MS/MS).

Bioanalytical Methodology for Metabolite Identification. The separation of metabolites was achieved at ambient temperature on a Kromasil C4 100A column (3.5 µm, 150 x 2.0 mm; Phenomenex, Torrance, CA) by reverse phase chromatography. The mobile phase consisted of 0.1% formic acid (solvent A) and acetonitrile (solvent B) and was delivered at 0.200 ml/min. A gradient was used to separate **3** and its metabolites as well as conjugates derived from trapping of reactive intermediates with exogenous nucleophiles. The initial composition of solvent B was maintained at 1% for 10 min and then increased in a linear manner as follows: 30% at 28 min; 50% at 30 min, and 90% at 35 min. It was then maintained at 90% for up to 37 min and then decreased to 1% in the next 3 min. The column was allowed to equilibrate at 1% solvent B for 5 min before the next injection. The HPLC effluent going to the mass spectrometer was directed to waste through a divert valve for the initial 5 min after sample injection. Mass spectrometric analyses were performed on a ThermoFinnigan Deca XP ion trap mass spectrometer, which was interfaced to an Agilent HP-1100 HPLC system (Agilent Technologies, Palo Alto, CA) and equipped with an electrospray ionization source. The values for electrospray ionization were as follows: capillary temperature, 270°C; spray voltage, 4.0 kV; capillary voltage, 4.0 V; sheath gas flow rate, 90; and auxiliary gas flow rate, 30. The mass spectrometer was operated in a positive ion mode with data-dependent scanning. The ions were monitored over a full mass range of *m*/*z* 100 to 1000. For a full scan, the automatic gain control was set at 5.0×10^8, maximum ion time was 100 ms, and the number of microscans was set at 3. For MS^n scanning, the automatic gain control 1.0 x

Downloaded from dmd.aspetjournals.org at ASPET Journals on May 23, 2024

DMD Fast Forward. Published on March 7, 2007 as DOI: 10.1124/dmd.106.013649
This article has not been copyedited and formatted. The final version may differ from this version.

10^8, maximum ion time was 400 ms, and the number of microscans was set at 2. For data-dependent scanning, the default charge-state was 1, default isolation width was 3.0, and normalized collision energy was 45.0. Metabolites were identified by comparing $t = 0$ samples to $t = 60$ min samples (with or without NADPH cofactor), and structural information was generated from collision-induced dissociation (CID) spectra of the corresponding protonated molecular ions and/or comparison with synthetic standards. Apart from full scan analysis, methoxylamine conjugate formation for **3** was also assessed by multiple reaction monitoring (MRM) of the anticipated mass transition corresponding to the loss of the 3-chlorobenzyl moiety (loss of 125 mass units) from the parent molecular ion of the respective amine conjugates.

Results

Genetic Toxicological Evaluations. The genetic safety of **3** was evaluated using the *Salmonella* reverse mutation assay. To simulate the effect of drug metabolizing enzymes in this system, the assay also included a segment where the cells were exposed to Aroclor 1254-induced rat liver S-9 mixture. To cover a broad spectrum of mutagenic mechanisms, a set of 4 commonly used tester strains TA98, TA100, TA1535 and TA1537 were utilized to evaluate mutagenicity of **3**. The exposure of *Salmonella* cells with **3** in the presence of S9 and NADPH co-factor resulted in a dose dependent and statistically significant increase ($p < 0.05$) of reverse mutations in strains TA100 and TA1537 (Figure 2, panel A). There was no increase observed in strains TA98 and TA1535. The dose response relationship exhibited a bell shape curve with maximum effect 5.5- and 3-fold observed at 0.633 mg/plate for TA100 and TA1537, respectively. The decreased incidence of reverse mutations at higher concentrations could be explained by a general

Downloaded from dmd.aspetjournals.org at ASPET Journals on May 23, 2024

DMD Fast Forward. Published on March 7, 2007 as DOI: 10.1124/dmd.106.013649
This article has not been copyedited and formatted. The final version may differ from this version.

cytotoxicity of **3** toward the *Salmonella* cells. The cytotoxicity of **3** was confirmed by reduced background lawn of bacterial cells. In contrast, treatment of *Salmonella* cells with **3** in the absence of S-9 and NADPH did not produce any significant increase of reverse mutations (Figure 2, panel B). This observation suggests that a metabolite of **3** is responsible for the mutagenic effects.

To assess whether the increased incidence of reverse mutations in the *Salmonella* assay is a consequence of covalent modification of DNA by a reactive metabolite of **3**, [^{14}C]-**3** was synthesized (see Figure 1) and reacted with calf thymus DNA in the presence or absence of metabolic activation system. The well-established reaction of [^{14}C]-benzo[a]pyrene with calf thymus DNA in the presence of metabolic activation (Szeliga and Dipple, 1998) was also included in this analysis as a positive control. Treatment of calf thymus DNA with [^{14}C]-benzo[a]pyrene led to a ~ 6-7-fold increase of DNA-bound radioactivity over the vehicle control or samples without aroclor 1254-induced rat liver S-9 (Table 1). Treatment of calf thymus DNA with [^{14}C]-**3** in absence of S-9 or presence of S-9 fraction without NADPH co-factor resulted in ~ 2-fold increase of radioactivity over the background levels. In contrast, inclusion of complete S9/NADPH activation system resulted in dose dependent increase of the covalently bound radioactivity over the DNA samples treated with [^{14}C]-**3** in absence of S9 or presence of S-9 fraction without co-factor (see Table 1).

Reactive Metabolite Trapping Studies. LC-MS/MS analysis of S-9 incubations containing **3**, an NADPH-regenerating system and methoxylamine led to the detection of a single conjugate **6** (MH^+ = 350) (Figure 3, panel B) that eluted after the parent compound (Figure 3, panel C). The methoxylamine conjugate **6** was detected in the full

Downloaded from dmd.aspetjournals.org at ASPET Journals on May 23, 2024

DMD Fast Forward. Published on March 7, 2007 as DOI: 10.1124/dmd.106.013649
This article has not been copyedited and formatted. The final version may differ from this version.

scan mode and in the MRM mode monitoring for the mass transition 350 → 125, which represents the loss of the 3-chlorobenzyl group from the anticipated mass of **6**. The observed molecular ion (MH^+ = 350 Da) of **6** was consistent with the addition of one molecule of methoxylamine to **3**. The formation of **6** was abolished when the NADPH-regenerating system (Figure 3, panel A) and/or methoxylamine were omitted from the incubations.

The product ion spectrum obtained by CID of the MH^+ at m/z 350 for the methoxylamine conjugate **6** and at m/z 305 for parent piperazine **3** is shown in Figure 4 panels A and B, respectively. The presence of the fragment ion at m/z 125 in the mass spectrum of **3** and **6** established that the structural integrity of the 3-chlorobenzyl group in **3** was maintained. MS^3 fragmentation of m/z 303 (arising from elimination of methoxylamine) afforded additional diagnostic fragment ions at m/z 262 and m/z 178, respectively. The presence of the fragment ion at m/z 262 in the mass spectrum of **3** and **6** suggested that the pyrazine ring plus a portion of the piperazine ring containing the internal nitrogen was also unaltered. Based on these fragment ions, a proposed structure for **6** that is consistent with the observed mass spectrum are shown in Figure 4, panel A. Methoxylamine conjugate **6** has the potential to exist in equilibrium as the ring closed or ring opened forms. Furthermore, while we have elected to arbitrarily depict the site of methoxylamine attachment to the carbon α to the secondary piperazine nitrogen, it is quite possible that the conjugation can occur on the carbon α to the tertiary piperazine nitrogen. The mass spectral characteristics of **6** do not provide additional insight into the site of methoxylamine attachment and conjugate **6** proved to be unstable towards purification for NMR studies.

Downloaded from dmd.aspetjournals.org at ASPET Journals on May 23, 2024

DMD Fast Forward. Published on March 7, 2007 as DOI: 10.1124/dmd.106.013649
This article has not been copyedited and formatted. The final version may differ from this version.

Full scan LC-MS/MS analysis of S-9 incubations containing **3**, an NADPH-regenerating system and potassium cyanide also led to the detection of a single conjugate **7** (MH^+ = 346, retention time (R_t) = 28 min) (Figure 5, panel A). The observed molecular ion (MH^+ = 346 Da) of **7** was consistent with the addition of one molecule of cyanide to a monohydroxylated metabolite of **3**. The formation of **7** was abolished when the NADPH-regenerating system and/or potassium cyanide were omitted from the incubations (data not shown). The product ion spectrum obtained by CID of the MH^+ at m/z 346 for the cyano conjugate **7** is shown in Figure 5 panel B. MS^3 fragmentation of m/z 319 (arising from elimination of cyanide) (Figure 5, panel C) afforded additional diagnostic fragment ions at m/z 248, 194 and 178, respectively. The fragment ions at m/z 194 and 178 suggested that the 3-chlorobenzyl portion in the conjugate was intact and that hydroxylation and subsequent cyanide addition had occurred on the pyrazinylpiperazine motif. Furthermore, the fragment ion at m/z 248 ruled out the internal tertiary piperazine nitrogen and the pyrazine ring as the sites of modification. A proposed structure for **7** that is consistent with the observed mass spectrum is shown in Figure 5.

Full scan LC-MS/MS analysis of S-9 incubations containing **3**, an NADPH-regenerating system and glutathione led to the detection of a single conjugate **8** (MH^+ = 448, R_t = 16.3 min) with a mass pattern corresponding to a monochlorinated species (Figure 6, panel A). The product ion spectrum obtained by CID of the MH^+ at m/z 448 produced fragment ions at m/z 373, 319 and 141 (Figure 6, panel B). The presence of the fragment ion at m/z 141 was consistent with the addition of 16 Da to the fragment ion at m/z 125 suggesting that glutathione conjugate **8** was derived from a monohydroxylated-3-chlorobenzyl fragment of piperazine **3**. The presence of the 3-chlorobenzyl ring of **3** in

Downloaded from dmd.aspetjournals.org at ASPET Journals on May 23, 2024

DMD Fast Forward. Published on March 7, 2007 as DOI: 10.1124/dmd.106.013649
This article has not been copyedited and formatted. The final version may differ from this version.

the structure of **8** was also consistent with the observed chlorine isotope pattern (see Figure 6, panel A, inset). The fragment ions at m/z 373 and m/z 319 were derived from loss of the glycine and glutamic acid components of glutathione (Baillie and Davis, 1993). A proposed structure that is consistent with the observed molecular weight is shown in Figure 6. While the regiochemistry of hydroxylation in **8** is shown to be at the position *para* to the benzylic carbon in Figure 6, it is possible that the hydroxylation could occur on the *ortho* position on the aromatic ring.

Effect of Exogenously Added Nucleophiles on the Mutagenic Response of 3 in the Salmonella Assay. Following incubation of **3** (0.5 mg/plate) with tester strain TA100 in the presence of Aroclor 1254-induced rat liver S-9 protein and NADPH co-factor, a 6.4-fold increase in reverse mutations was observed. Addition of methoxylamine (1 mM) led to a statistically significant reduction in reverse mutations (~ 1.8-fold increase over control, $p < 0.05$) (Table 2). While reductions in reverse mutations were also observed upon inclusion of glutathione (1 mM), the decrease was not statistically significant over control (revertant count (- glutathione) = 941 ± 85; revertant count (+ glutathione) = 684 (mean of two experiments).

General Metabolic Profile of Piperazine (3) in NADPH-Supplemented Aroclor 1254-induced Rat Liver S-9 Protein. Figure 7, panel A depicts a full scan analysis of the various metabolites of piperazine **3** observed in Aroclor 1254-induced rat liver S-9 protein in a NADPH-dependent fashion. A total of 8 metabolites eluting before parent were observed. The major metabolite **M7** eluted at R_t of 24.5 min and displayed a molecular ion (MH^+) at 279, which was 26 Da lower than the molecular mass of the parent compound **3**. The mass spectral characteristics of **M7** (Figure 7, panel B) are

Downloaded from dmd.aspetjournals.org at ASPET Journals on May 23, 2024

DMD Fast Forward. Published on March 7, 2007 as DOI: 10.1124/dmd.106.013649
This article has not been copyedited and formatted. The final version may differ from this version.

consistent with P450-mediated piperazine ring scission in **3** to yield the diamine metabolite **M7**. The retention time and mass spectral properties of **M7** were identical to the synthetic standard of the diamine metabolite **5**. The product ion spectra obtained by the CID of the MH^+ ions for the remainder of the metabolites provided some insight into their respective structures. For instance, the metabolite **M4** exhibited a molecular ion (MH^+) at 295, which indicated that **M4** was a monohydroxylated metabolite of **M7**. The mass spectrum of **M4** suggested that the site of monohydroxylation was on the 3-chlorophenyl ring (Figure 7, panel C). Metabolites **M1**, **M2** and **M5** were derived from monohydroxylation of parent **3** since their molecular mass (MH^+ = 321) represented the addition of 16 Da to the molecular ion of **3** (MH^+ = 305). The CID spectra of **M1** and **M5** indicated the presence of base fragment ions at m/z 193 and m/z 141suggesting that the pyrazinylpiperazine motif was intact and that the site of monohydroxylation was the 3-chlorophenyl ring in **3** (Figure 8). The CID spectra of **M2** revealed the presence of a base fragment ion at m/z 196 which is the addition of 16 Da to the ion fragment at m/z 179 in the mass spectrum of **3**. This observation suggested that the pyrazinylpiperazine group in **M2** had undergone monohydroxylation. The additional diagnostic ion fragments at m/z 293 and 278 leads us to speculate the pyrazine ring as the site of oxidation. The molecular ion (MH^+ = 337) of metabolite **M3** was consistent with dihydroxylation of **3**. The CID spectra of **M3** indicated the presence of a base fragment ion at m/z 209 that suggested that the one site of oxidation was the pyrazinylpiperazine group. The lack of additional diagnostic mass fragments leads us to speculate that the second site of oxidation is the 3-chlorophenyl ring in **3**.

Downloaded from dmd.aspetjournals.org at ASPET Journals on May 23, 2024

DMD Fast Forward. Published on March 7, 2007 as DOI: 10.1124/dmd.106.013649
This article has not been copyedited and formatted. The final version may differ from this version.

Metabolite **M6** (R_t = 22.1 min) exhibited a molecular ion (MH^+) at m/z 307, which was 2 mass units greater than the molecular weight of **3**. The mass spectrum of **M6** at m/z 307 revealed at fragment ion at *m/z* 289 in the MS^2 spectrum suggesting the loss of a water molecule (Figure 9). The fragment ion at *m/z* 289 was subjected to further fragmentation in the data dependant scanning mode. This spectrum gave major fragment ions at *m/z* 262, 246, 219, 164 and 125 as shown in Figure 9. The fragmentation pattern and the molecular ion led us to speculate that **M6** is derived from a unique piperazine ring opening pathway leading to the ring-contracted imidazolidinol isomers shown in Figure 9.

Finally, of great interest in the present context was the formation of metabolite **M8** that exhibited a molecular ion (MH^+) at 461, 156 Da higher than the observed MH^+ for the parent piperazine **3** and with a mass pattern consistent with a dichlorinated species. The formation of this metabolite was NADPH-dependent and drug-related since the CID spectrum of this metabolite (Figure 10) revealed the presence of a fragment ion at m/z 321 corresponding to mono-hydroxylated **3**. Likewise, the fragment ion at m/z 193 was also observed in the product ion spectra of mono-hydroxylated metabolites **M1** or **M5** suggesting that **M8** may be a derivative of **M1** and **M5**, which are hydroxylated on the 3-chlorobenzyl ring. Based on these observations, a proposed structure for **M8** is shown in Figure 10 in which the remaining 140 Da that are required to complete the structure (MH^+ 461 → m/z 321) are envisioned to arise from an additional 3-chloro-4-hydroxybenzyl motif. While the regiochemistry of hydroxylation in **M8** is shown to be at the position *para* to the benzylic carbon in Figure 10, it is possible that the hydroxylation could occur on the *ortho* position on the aromatic ring. An analog of **M8** that eluted at R_t

Downloaded from dmd.aspetjournals.org at ASPET Journals on May 23, 2024

DMD Fast Forward. Published on March 7, 2007 as DOI: 10.1124/dmd.106.013649
This article has not been copyedited and formatted. The final version may differ from this version.

~ 24.8 min and possessed an MH^+ at 445 was also detected in the reactions of **3** with S-9. The molecular weight of this metabolite was consistent with the addition of one molecule of **3** to the 3-chloro-4-hydroxybenzyl motif (data not shown). Finally, it is interesting to note that inclusion of glutathione (but not methoxylamine or cyanide) in the NADPH-supplemented rat S-9 led to a complete disappearance of the **M8** metabolite peak (data not shown).

Discussion

Despite the attractive in vitro and in vivo pharmacology of **3** as a selective 5-HT_{2C} agonist, further development of this compound as a potential drug candidate for the treatment of obesity was suspended due to the rat S-9/NADPH-dependent mutagenic response of **3** in the *Salmonella* assay and subsequent covalent binding of [^{14}C]-**3** to calf thymus DNA. The findings that both S-9 and NADPH co-factor were essential for the mutagenic response and the covalent binding to DNA strongly suggested that **3** is bioactivated by rat cytochrome P450 enzyme(s) to a reactive metabolite(s), which covalently adducts to a DNA base(s). In the *Salmonella* assay, **3** produced a significant increase of mutations only in strains TA100 and TA1537 that are known to be sensitive to mainly base-pair and frame-shift mutagens (Maron and Ames, 1984). This suggests that the putative mutagenic metabolite exhibits a structural DNA specificity.

Reactive metabolite trapping studies in NADPH-supplemented Aroclor 1254-induced rat S-9 incubations of **3** in the presence of amine, cyanide and glutathione nucleophiles led to the detection of conjugates of **3** with each of these trapping agents. This observation suggested that **3** was bioactivated to both hard and soft electrophilic intermediates capable of forming stable adducts with corresponding hard (methoxylamine

Downloaded from dmd.aspetjournals.org at ASPET Journals on May 23, 2024

DMD Fast Forward. Published on March 7, 2007 as DOI: 10.1124/dmd.106.013649
This article has not been copyedited and formatted. The final version may differ from this version.

and cyanide) and soft (glutathione) nucleophiles. The observed molecular ion of the methoxylamine and the cyanide conjugates of **3**, i.e., **6** and **7** were consistent with the addition of one molecule of methoxylamine to **3** and addition of one molecule of cyanide to mono-hydroxylated **3**, respectively. Furthermore, the mass spectrum of **6** and **7** suggested that the site of adduction of both the amine and the cyanide nucleophile occurred on the piperazine ring system. Overall, the in vitro reactive metabolite trapping studies using methoxylamine, the data on the covalent adduction of [^{14}C]-**3** to calf-thymus DNA and the observation that inclusion of methoxylamine in the Ames assay results in a statistically significant attenuation in the mutagenic response, strengthen the link between piperazine ring bioactivation and the mutagenic response with **3**. A bioactivation sequence is proposed in which initial P450-mediated hydroxylation on the carbon α to the secondary piperazine nitrogen in **3** would afford the unstable carbinolamine intermediate, which would spontaneously open to the electrophilic aldehyde intermediate (Figure 11, pathway a). Condensation of this carbonyl intermediate with methoxylamine would give rise to the Schiff base conjugate **6**, capable of existing in the ring-opened or ring closed forms. Alternately, a direct two-electron oxidation of the α-carbon-nitrogen bond in **3** will generate the electrophilic iminium intermediate (Figure 11, pathway b), which upon reaction with methoxylamine would also afford **6**. The proposed mechanism for the formation of the cyano conjugate **7** is shown in Figure 11, pathway c. Initial oxidation of the secondary piperazine nitrogen in **3** would furnish the hydroxylamine intermediate, which, upon a two-electron oxidation on the α-carbon-nitrogen bond would lead to the nitrone derivative capable of reacting with cyanide ion and generating conjugate **7** in a manner similar to that observed for related

Downloaded from dmd.aspetjournals.org at ASPET Journals on May 23, 2024

DMD Fast Forward. Published on March 7, 2007 as DOI: 10.1124/dmd.106.013649
This article has not been copyedited and formatted. The final version may differ from this version.

acyclic analogs (Kim et al., 1999; Clark and Carokill, 1975). Considering that exogenously added amine-trapping agents such as methoxylamine are well-established model nucleophilies for assessing the reactivity of hard electrophiles with DNA bases in vitro microsomal incubations (Ames et al., 1977; Schnetz-Boutaud et al., 2000; Chen et al., 1997; Chen et al., 1995), we further propose that the electrophilic aldehyde or iminium intermediate undergoes similar chemistry with an appropriate base in DNA leading to a mutagenic response. Besides these bioactivation mechanisms, there also exists the possibility of an additional pathway that would lead to an aldehyde intermediate capable of reacting with exogenously added nucleophiles including DNA. Thus, the P450-catalyzed piperazine ring scission in **3** to yield the diamine metabolite **5** would in theory result in the concomitant liberation of the electrophilic glyoxal (Figure 11, pathway d). The contribution of this pathway to the mutagenic response of **3** cannot be ruled out despite the lack of detection of the corresponding methoxylamine conjugate(s) of glyoxal in NADPH-supplemented rat S-9 (data not shown) and the observed incorporation of radioactivity into calf thymus DNA (^{14}C radiolabel was on the pyrazine motif). Finally, the observation that methoxylamine significantly decreases the mutagenic response of **3** suggests that this hard nucleophile effectively competes with DNA bases and scavenges electrophilic carbonyl intermediates derived from piperazine ring scission.

The formation of both the glutathione conjugate **8** and metabolite **M8** can be explained via a single bioactivation pathway (Figure 12). Thus, initial P450-catalyzed *ortho* or *para* aromatic hydroxylation (for the sake of simplicity, the bioactivation pathway is exemplified using the *para* isomer) would generate the mono-hydroxylated

Downloaded from dmd.aspetjournals.org at ASPET Journals on May 23, 2024

DMD Fast Forward. Published on March 7, 2007 as DOI: 10.1124/dmd.106.013649
This article has not been copyedited and formatted. The final version may differ from this version.

metabolite of **3** (either **M1** or **M2**), which possesses the ability to undergo elimination liberating a reactive quinone-methide intermediate that can undergo Michael addition with glutathione to afford **8**. It is interesting to point out that in the absence of exogenously added glutathione the secondary piperazine nitrogen in **3** and its monohydroxylated metabolite (most likely **M1** or **M2** based on the observation that hydroxylation occurred on the 3-chlorophenyl ring) was sufficiently nucleophilic towards reaction with the electrophilic quinone-methide. The formation of both **8** and **M8** is not altogether surprising considering that the reaction of sulhydryl, cyclic and acyclic amine nucleophiles (Modica et al., 2001; Bolton et al., 1997) and DNA bases (Wang et al., 2005; Bodell et al., 1998; Bolton et al., 1994) with electrophilic quinone-methide intermediates liberated from the bioactivation of xenobiotics including drugs is well known.

From a structure-mutagenicity relationship point of view, the P450-catalyzed formation of the diamine metabolite **5**, the methoxylamine conjugate **6** the cyano conjugate **7** and the metabolite **M8** suggests that electrophilic carbonyl/iminium intermediates (derived from the piperazine ring metabolism) as well as the quinone-methide (derived from the bioactivation of the 3-chlorobenzyl group) possess the ability to react with DNA. While evidence linking the involvement of the aldehyde intermediate derived from the piperazine ring scission in **3** towards reaction with DNA is strengthened on the basis of the DNA covalent binding studies and the decrease in mutagenic response in the *Salmonella* Ames assay following co-incubation with methoxylamine, additional studies will be needed to decipher the contribution of other reactive species especially the quinone-methide in the mutagenic response of **3**. Structure-toxicity relationship studies

Downloaded from dmd.aspetjournals.org at ASPET Journals on May 23, 2024

DMD Fast Forward. Published on March 7, 2007 as DOI: 10.1124/dmd.106.013649
This article has not been copyedited and formatted. The final version may differ from this version.

are in progress and will involve an assessment of the mutagenic potential of analogs of **3** specifically designed to avoid quinone-methide formation while maintaining the rest of the chemical architecture (pyrazinyl-piperazine) constant. Likewise, a parallel effort involving the replacement of the secondary piperazine nitrogen with suitable bioisosteres and/or introduction of α-carbon alkyl substituents on the piperazine ring in **3** while maintaining the 3-chlorobenzyl motif constant is also in the works. These studies will be reported in due course.

Downloaded from dmd.aspetjournals.org at ASPET Journals on May 23, 2024

DMD Fast Forward. Published on March 7, 2007 as DOI: 10.1124/dmd.106.013649
This article has not been copyedited and formatted. The final version may differ from this version.

References

Ames AA, Nelson SD, Lovenberg W and Sasame HA (1977) Metabolic activation of para-chloroamphetamine to a chemically reactive metabolite. *Commun Psychopharmacol* **1:**455-460.

Baillie TA and Davis MR (1993) Mass spectrometry in the analysis of glutathione conjugates. *Biol. Mass Spectrom* **22:**319-325.

Bickerdike MJ (2003) 5-HT2C receptor agonists as potential drugs for the treatment of obesity. *Curr Top Med Chem* **3:**885-897.

Bodell WJ, Ye Q, Pathak DN and Pongracz K (1998) Oxidation of eugenol to form DNA adducts and 8-hydroxy-2'-deoxyguanosine: role of quinone methide derivative in DNA adduct formation. *Carcinogenesis* **19:**437-443.

Bolton JL, Turnipseed SB and Thompson JA (1997) Influence of quinone methide reactivity on the alkylation of thiol and amino groups in proteins: studies utilizing amino acid and peptide models. *Chem Biol Interact* **107:**185-200.

Bolton JL, Acay NM and Vukomanovic V (1994) Evidence that 4-allyl-o-quinones spontaneously rearrange to their more electrophilic quinone methides: potential bioactivation mechanism for the hepatocarcinogen safrole. *Chem Res Toxicol* **7:**443-450.

Chen LJ, Hecht SS and Peterson LA (1995) Identification of cis-2-butene-1,4-dial as a microsomal metabolite of furan. *Chem Res Toxicol* **8:**903-906.

Chen LJ, Hecht SS and Peterson LA (1997) Characterization of amino acid and glutathione adducts of cis-2-butene-1,4-dial, a reactive metabolite of furan. *Chem Res Toxicol* **10:**866-874.

Downloaded from dmd.aspetjournals.org at ASPET Journals on May 23, 2024

DMD Fast Forward. Published on March 7, 2007 as DOI: 10.1124/dmd.106.013649
This article has not been copyedited and formatted. The final version may differ from this version.

Clark NG and Carokill E (1977) Reaction between cyanide ion and nitrones. Novel imidazole synthesis. *Tetrahedron Lett* **31:**2717-2720.

Dunlop J, Sabb AL, Mazandarani H, Zhang J, Kalgaonker S, Shukhina E, Sukoff S, Vogel RL, Stack G, Schechter L, Harrison BL and Rosenzweig-Lipson S (2005) WAY-163909 [(7bR,10aR)-1,2,3,4,8,9,10,10a-octahydro-7bH-cyclopenta-[b][1,4]diazepino[6,7,1hi]indole], a novel 5-hydroxytryptamine 2C receptor-selective agonist with anorectic activity. *J Pharmacol Exp Ther* **313:**862-869.

Heisler LK, Chu HM and Tecott LH (1998) Epilepsy and obesity in serotonin 5-HT2C receptor mutant mice. *Ann N Y Acad Sci* **861:**74-78.

Hoyer D, Hannon JP and Martin GR (2002) Molecular, pharmacological and functional diversity of 5-HT receptors. *Pharmacol Biochem Behav* **71:**533-554.

Kim BS and Margolin BH (1999) Prediction of rodent carcinogenicity utilizing a battery of in vitro and in vivo genotoxicity tests. *Environ Mol Mutagen* **34:**297-304.

Kim T-R, Kim Y-H and Pyun S-Y (1999) Kinetic studies on the addition of potassium cyanide to α,N-diphenylnitrone. *Bull Korean Chem Soc* **20:**712-714.

Kimura Y, Hatanaka K, Naitou Y, Maeno K, Shimada I, Koakutsu A, Wanibuchi F and Yamaguchi T (2004) Pharmacological profile of YM348, a novel, potent and orally active 5-HT2C receptor agonist. *Eur J Pharmacol* **483:**37-43.

Maron DM and Ames BN (1984) Revised methods for the Salmonella mutagenicity test. *Mutat Res* **113:**173-215.

Masand PS (2000) Weight gain associated with psychotropic drugs. *Expert Opin Pharmacother* **1:**377-389.

Downloaded from dmd.aspetjournals.org at ASPET Journals on May 23, 2024

DMD Fast Forward. Published on March 7, 2007 as DOI: 10.1124/dmd.106.013649
This article has not been copyedited and formatted. The final version may differ from this version.

Modica E, Zanaletti R, Freccero M and Mella M (2001) Alkylation of amino acids and glutathione in water by o-quinone methide. Reactivity and selectivity. *J Org Chem* **66:**41-52.

Muller L, Kikuchi Y, Probst G, Schechtman L, Shimada H, Sofuni T, Tweats D (1999) ICH-harmonised guidances on genotoxicity testing of pharmaceuticals: evolution, reasoning and impact. *Mutation Res* **436:**195-225.

Nonogaki K, Strack AM, Dallman MF and Tecott LH (1998) Leptin-independent hyperphagia and type 2 diabetes in mice with a mutated serotonin 5-HT2C receptor gene. *Nat Med* **4:**1152-1156.

Schnetz-Boutaud N, Daniels JS, Hashim MF, Scholl P, Burrus T and Marnett LJ (2000) Pyrimido[1,2-alpha]purin-10(3H)-one: a reactive electrophile in the genome. *Chem Res Toxicol* **13:**967-970.

Szeliga J and Dipple A (1998) DNA adduct formation by polycyclic aromatic hydrocarbon dihydrodiol epoxides. *Chem Res Toxicol* **11:**1-11.

Tecott LH, Sun LM, Akana SF, Strack AM, Lowenstein DH, Dallman MF and Julius D (1995) Eating disorder and epilepsy in mice lacking 5-HT2c serotonin receptors. *Nature* **374:**542-546.

Vickers SP and Dourish CT (2004) Serotonin receptor ligands and the treatment of obesity. *Curr Opin Invest Drugs* **5:**377-388.

von Meyenburg C, Langhans W and Hrupka BJ (2003) Evidence that the anorexia induced by lipopolysaccharide is mediated by the 5-HT2C receptor. *Pharmacol Biochem Behav* **74:**505-512.

Downloaded from dmd.aspetjournals.org at ASPET Journals on May 23, 2024

DMD Fast Forward. Published on March 7, 2007 as DOI: 10.1124/dmd.106.013649
This article has not been copyedited and formatted. The final version may differ from this version.

Zeiger E (1998) Identification of rodent carcinogens and noncarcinogens using genetic toxicity tests: premises, promises, and performance. *Regul Toxicol Pharmacol* **28:**85-95.

Downloaded from dmd.aspetjournals.org at ASPET Journals on May 23, 2024

DMD Fast Forward. Published on March 7, 2007 as DOI: 10.1124/dmd.106.013649
This article has not been copyedited and formatted. The final version may differ from this version.

FIGURE LEGENDS

FIG. 1. Synthetic scheme for the title compounds used in the study.

FIG. 2. Evaluation of piperazine **3** in the *Salmonella* reverse mutation assay. The mutagenic potential of **3** was tested using *Salmonella* tester strains TA100 (□), TA98 (■), TA 1535 (●)and TA 1537 (▲). The experiments were performed in presence (A) and absence (B) of metabolic activation (aroclor 1254-induced rat liver S-9 mixture and a NADPH regenerating system). The data represent average of 3 independent experiments ±SEM. Statistical significance was evaluated using t-test, *, $p \leq 0.05$.

FIG. 3. Extracted ion chromatogram (MRM mode 350 → 125) of the methoxylamine conjugate **6** (R_t = 14.40 min) of piperazine derivative **3** (panel B) following incubation of **3** with NADPH-supplemented aroclor 1254-induced rat liver S-9 protein in the presence of excess methoxylamine. Panel A depicts the lack of conjugate formation in the absence of NADPH and Panel C reflects the extracted ion chromatogram (MRM mode 305 → 125) of the parent piperazine **3** (R_t = 13.82 min) in these incubations.

FIG. 4. Product ion spectra obtained by CID of the MH^+ ion (m/z 350) of the methoxylamine conjugate **6** (R_t = 14.40 min) (Panel A). Panel B depicts the product ion spectra obtained by CID of the MH^+ ion (m/z 305) of the parent piperazine **3** (R_t = 13.82 min). The origins of the diagnostic ions are as indicated.

Downloaded from dmd.aspetjournals.org at ASPET Journals on May 23, 2024

DMD Fast Forward. Published on March 7, 2007 as DOI: 10.1124/dmd.106.013649
This article has not been copyedited and formatted. The final version may differ from this version.

FIG. 5. Extracted ion chromatogram of the cyano conjugate **7** (R_t = 28.00 min) of piperazine derivative **3** following incubation of **3** with NADPH-supplemented aroclor 1254-induced rat liver S-9 protein in the presence of excess potassium cyanide (panel A). Panel B depicts the product ion spectrum obtained by CID of the MH^+ ion (m/z 346) of **7** and Panel C depicts the MS^3 spectrum of fragment ion m/z 319 observed in the product ion spectrum of **7**.

FIG. 6. Extracted ion chromatogram of the glutathione conjugate **8** (R_t = 16.3 min) of piperazine derivative **3** following incubation of **3** with NADPH-supplemented aroclor 1254-induced rat liver S-9 protein in the presence of excess glutathione (panel A). Panel B depicts the product ion spectrum obtained by CID of the MH^+ ion (m/z 448) of **8**. The origins of the characteristic ions are as indicated.

FIG. 7. Total ion chromatogram (panel A) of the various metabolites of **3** following incubation in NADPH-supplemented aroclor 1254-induced rat liver S-9 protein. Panel B depicts the product ion spectrum obtained by CID of the MH^+ ion (m/z 279) of the major metabolite of **3**, i.e., **M7**. Panel C depicts the product ion spectrum obtained by CID of the MH^+ ion (m/z 295) of the **M4**, the monohydroxylated metabolite of **M7**.

FIG. 8. Product ion spectra obtained by the CID of the MH^+ ions of the **M1**-**M3** and **M5** metabolites of **3** in NADPH-supplemented aroclor 1254-induced rat liver S-9 protein.

FIG. 9. Product ion spectra obtained by the CID of the MH^+ ion of the **M6** metabolite of **3** in NADPH-supplemented aroclor 1254-induced rat liver S-9 protein.

Downloaded from dmd.aspetjournals.org at ASPET Journals on May 23, 2024

DMD Fast Forward. Published on March 7, 2007 as DOI: 10.1124/dmd.106.013649
This article has not been copyedited and formatted. The final version may differ from this version.

FIG. 10. Product ion spectra obtained by the CID of the MH^+ ion of the **M8** metabolite of **3** in NADPH-supplemented aroclor 1254-induced rat liver S-9 protein.

FIG. 11. Proposed P450-catalyzed bioactivation pathways involving the piperazine ring in **3**.

FIG. 12. Proposed P450-catalyzed bioactivation pathways involving the 3-chlorobenzyl ring in **3**.

Downloaded from dmd.aspetjournals.org at ASPET Journals on May 23, 2024

DMD Fast Forward. Published on March 7, 2007 as DOI: 10.1124/dmd.106.013649
This article has not been copyedited and formatted. The final version may differ from this version.

TABLE 1

*S-9/NADPH-dependent covalent binding of [^{14}C]-piperazine analog **3** to calf-thymus DNA*

Incubation	Test I Mean DPM[a]/20 μg DNA	Test II Mean DPM[a]/20 μg DNA
Vehicle (DMSO)	35 (34, 35)	23 (24, 24, 22)
Benzo[a]pyrene (100 μM) - S9	43 (37, 48)	20 (19, 21, 20)
Benzo[a]pyrene (100 μM) + complete system	302 (305, 299)	137 (138, 137, 136)
3 (0.5 μM) - S9	51 (54, 47)	52 (48, 48, 59)
3 (0.5 μM) + incomplete S-9	40 (39,41)	42 (42, 41, 43)
3 (0.5 μM) + complete S-9	166 (171, 160)	100 (95, 104)
3 (0.5 μM) + complete S-9	105 (104, 106)	124 (126, 121)
3 (5.0 μM) + complete S-9	495 (490,501)	462 (472, 451)

Calf thymus DNA (1 mg/ml) was incubated with either vehicle (DMSO), [^{14}C]-benzo[a]pyrene (100 μM) (positive control), or [^{14}C]-**3** at 0.5 and 5.0 μM for 3 hr at 37° C. The DNA-bound compound was quantified using scintillation counting. Incubations were carried out either without metabolic activation (-S9), with complete activation system (+ S9 and NADPH co-factor), or incomplete S-9 activation system that lacked NADPH or NADP. NADPH was used in test I and NADPH regenerating system was used in test II. [a] mean DPM represents average from two to three separate experiments.

Downloaded from dmd.aspetjournals.org at ASPET Journals on May 23, 2024

DMD Fast Forward. Published on March 7, 2007 as DOI: 10.1124/dmd.106.013649
This article has not been copyedited and formatted. The final version may differ from this version.

TABLE 2

*Effect of exogenously added methoxylamine on the S-9/NADPH-dependent mutagenic response of **3** in the Salmonella Ames assay using tester strain TA100*

Condition	Glutathione (1 mM)	Methoxylamine (1 mM)	Revertant Count	Fold Increase
vehicle + S-9/NADPH	-	-	148 ± 4.9	1.0
3 + S-9/NADPH	-	-	941 ± 85	6.4*
3 + S-9/NADPH	-	+	134 ± 22	1.8*
3 + S-9/NADPH	+	-	684[§]	1.3

The values represent average of three independent experiments ± SEM. [§]Mean of 2 experiments. The statistical significance of revertant counts increases over solvent treated control in each set of experiments was evaluated using t-test (*, $p \leq 0.05$).

Downloaded from dmd.aspetjournals.org at ASPET Journals on May 23, 2024

Figure 1

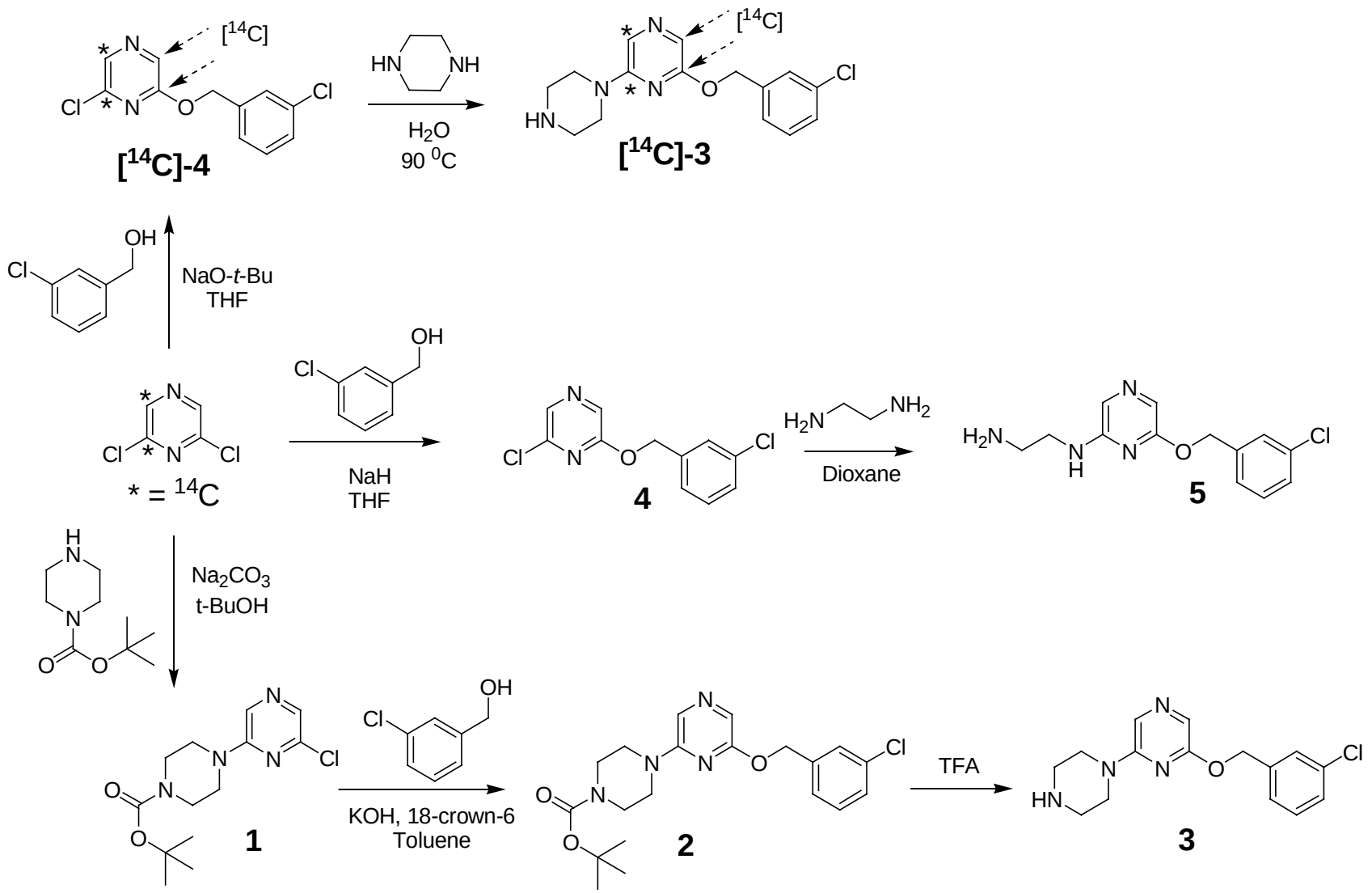

DMD Fast Forward. Published on March 7, 2007 as DOI: 10.1124/dmd.106.013649
This article has not been copyedited and formatted. The final version may differ from this version.

Downloaded from dmd.aspetjournals.org at ASPET Journals on May 23, 2024

Figure 2

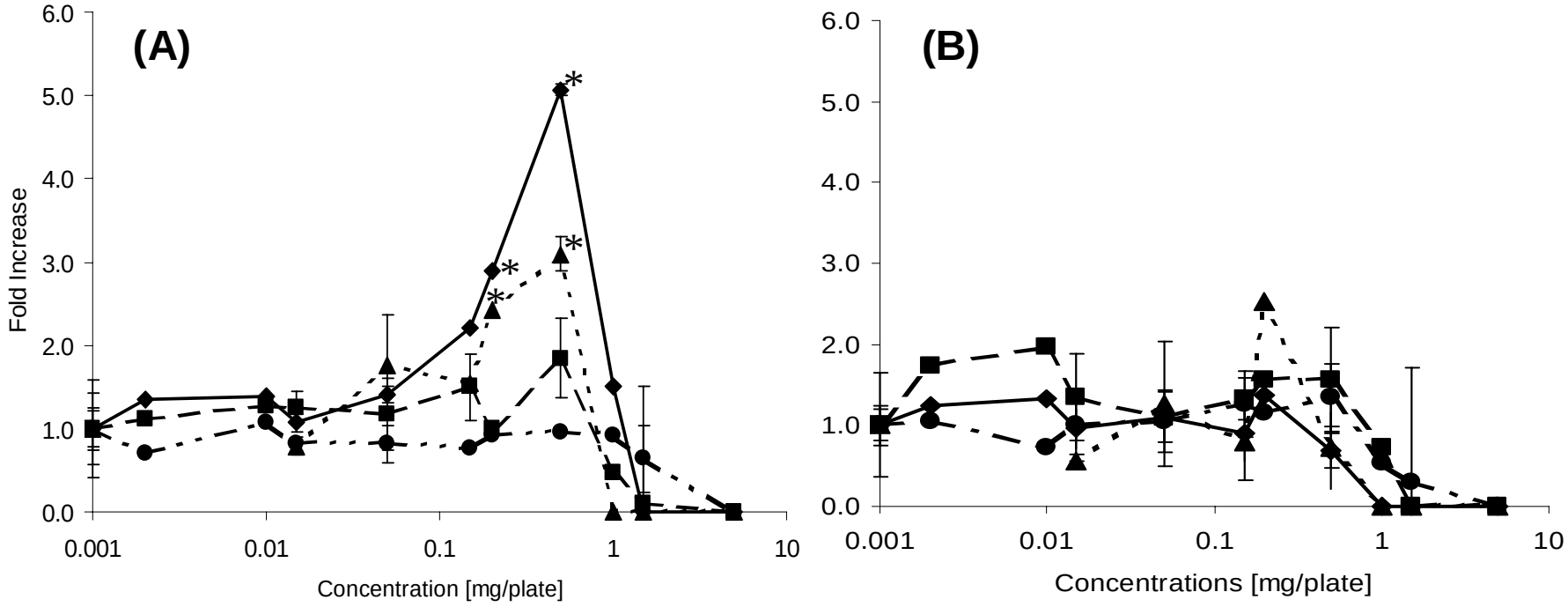

DMD Fast Forward. Published on March 7, 2007 as DOI: 10.1124/dmd.106.013649
This article has not been copyedited and formatted. The final version may differ from this version.

Downloaded from dmd.aspetjournals.org at ASPET Journals on May 23, 2024

Figure 3

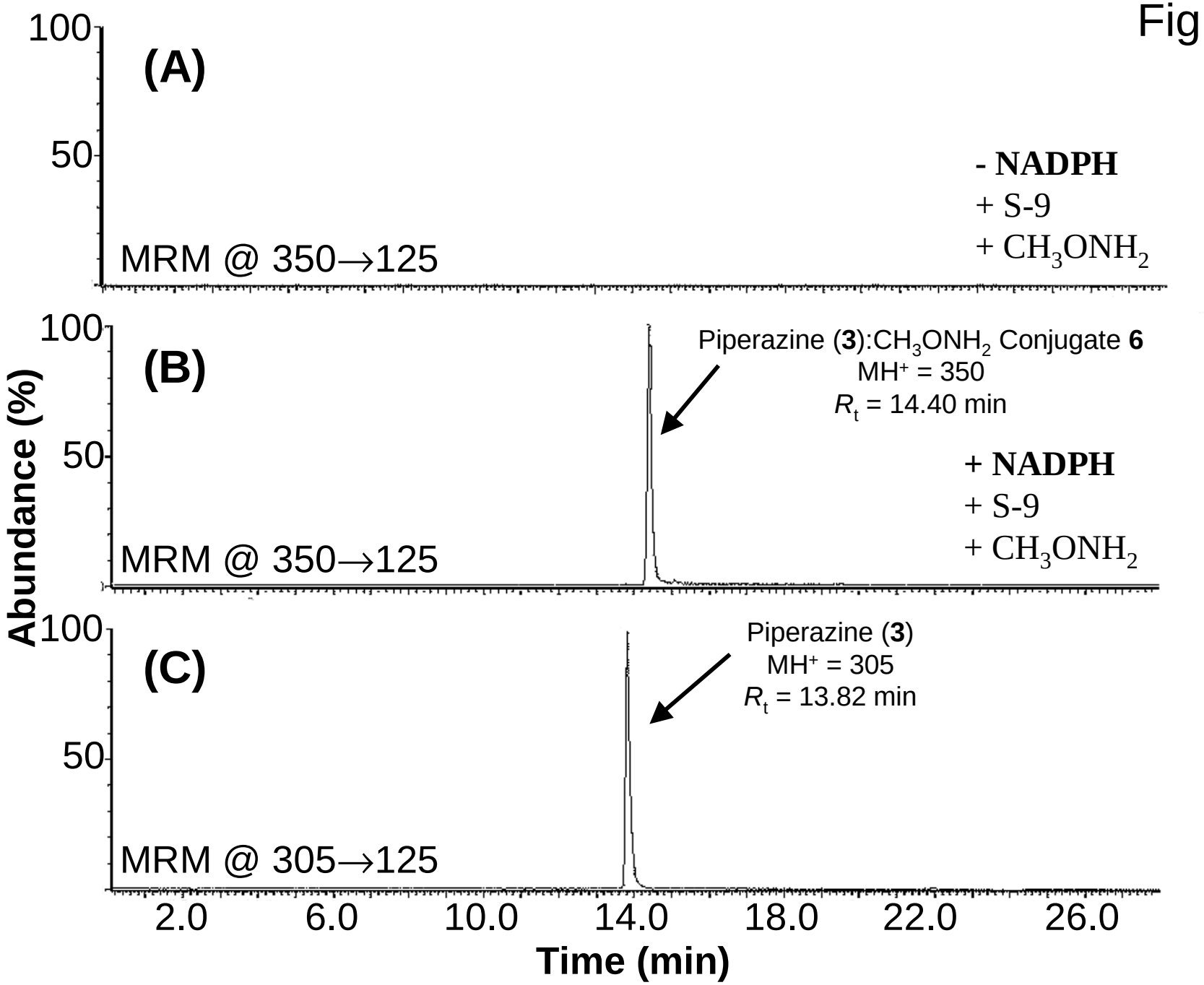

DMD Fast Forward. Published on March 7, 2007 as DOI: 10.1124/dmd.106.013649
This article has not been copyedited and formatted. The final version may differ from this version.

Downloaded from dmd.aspetjournals.org at ASPET Journals on May 23, 2024

Figure 4

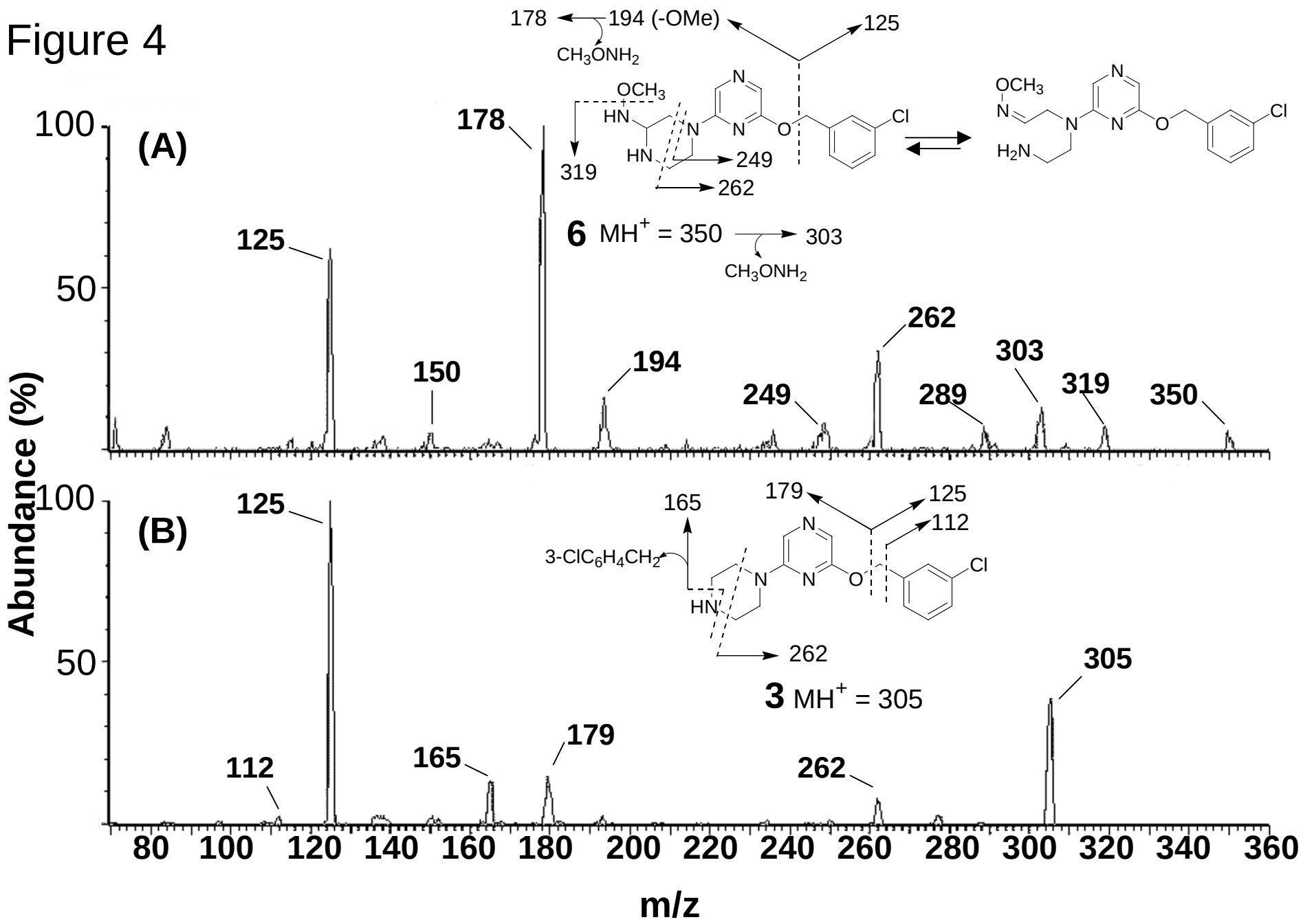

DMD Fast Forward. Published on March 7, 2007 as DOI: 10.1124/dmd.106.013649
This article has not been copyedited and formatted. The final version may differ from this version.

Downloaded from dmd.aspetjournals.org at ASPET Journals on May 23, 2024

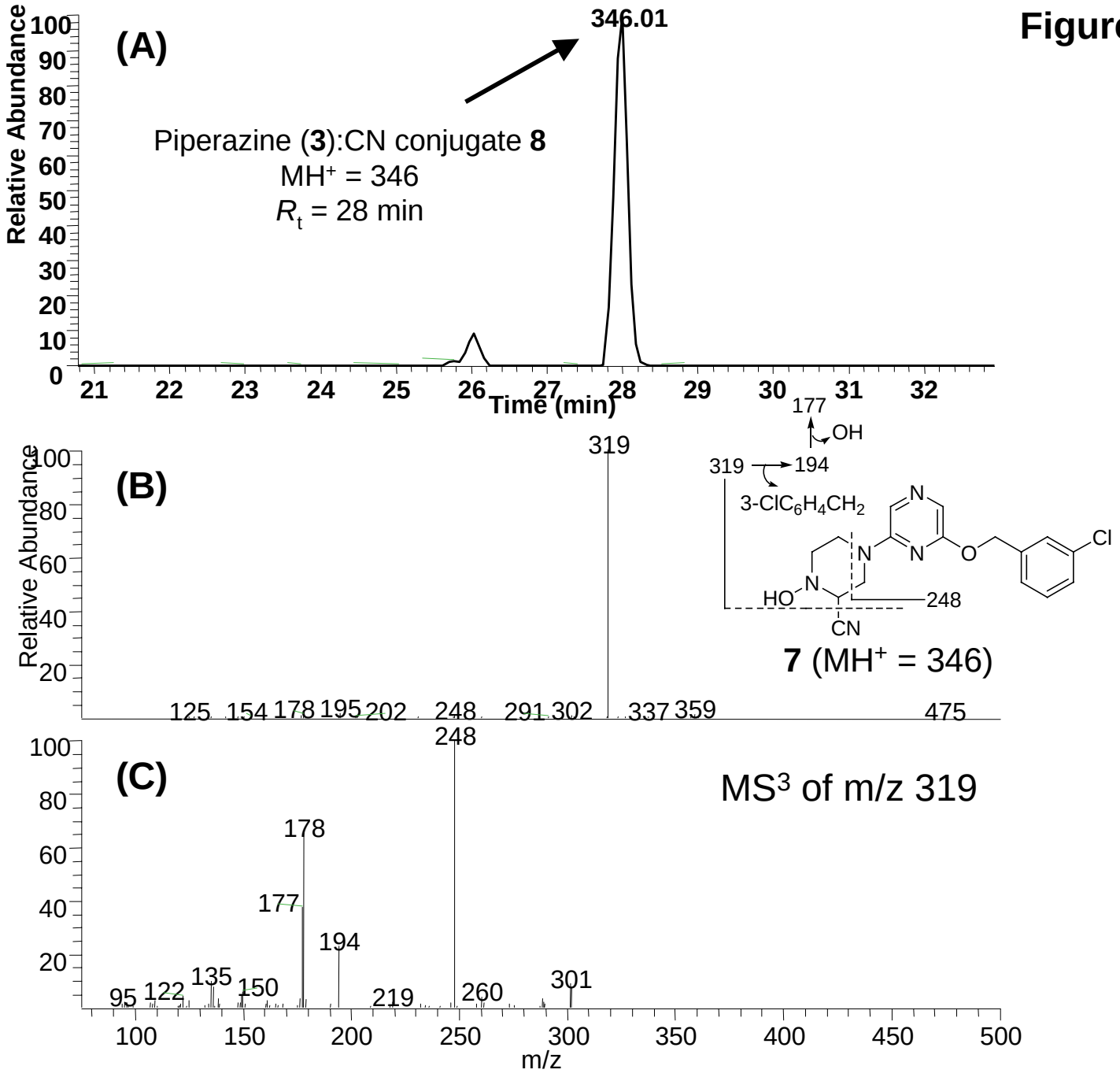

Figure 5

DMD Fast Forward. Published on March 7, 2007 as DOI: 10.1124/dmd.106.013649
This article has not been copyedited and formatted. The final version may differ from this version.

Downloaded from dmd.aspetjournals.org at ASPET Journals on May 23, 2024

DMD Fast Forward. Published on March 7, 2007 as DOI: 10.1124/dmd.106.013649
This article has not been copyedited and formatted. The final version may differ from this version.

Figure 6

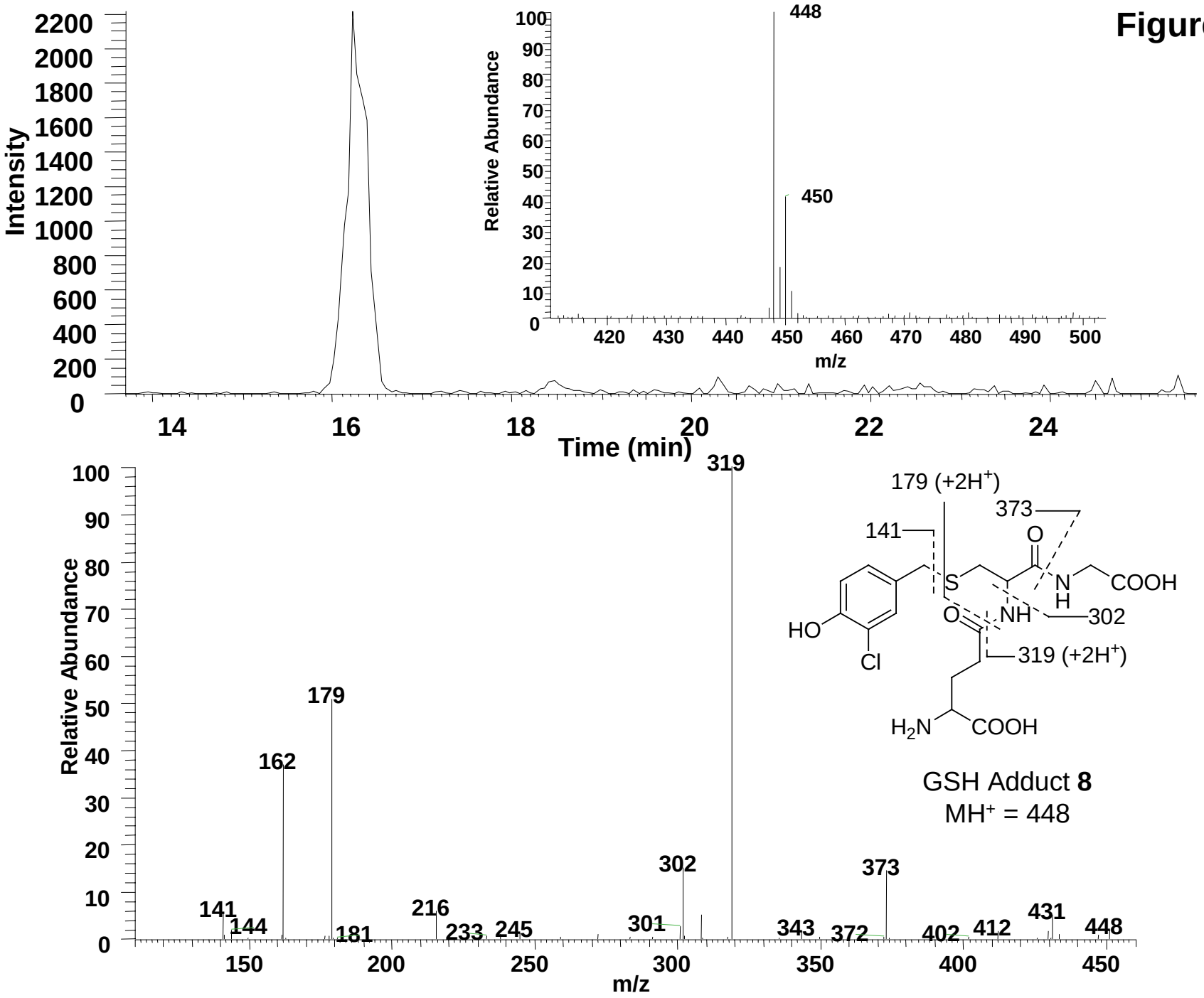

Downloaded from dmd.aspetjournals.org at ASPET Journals on May 23, 2024

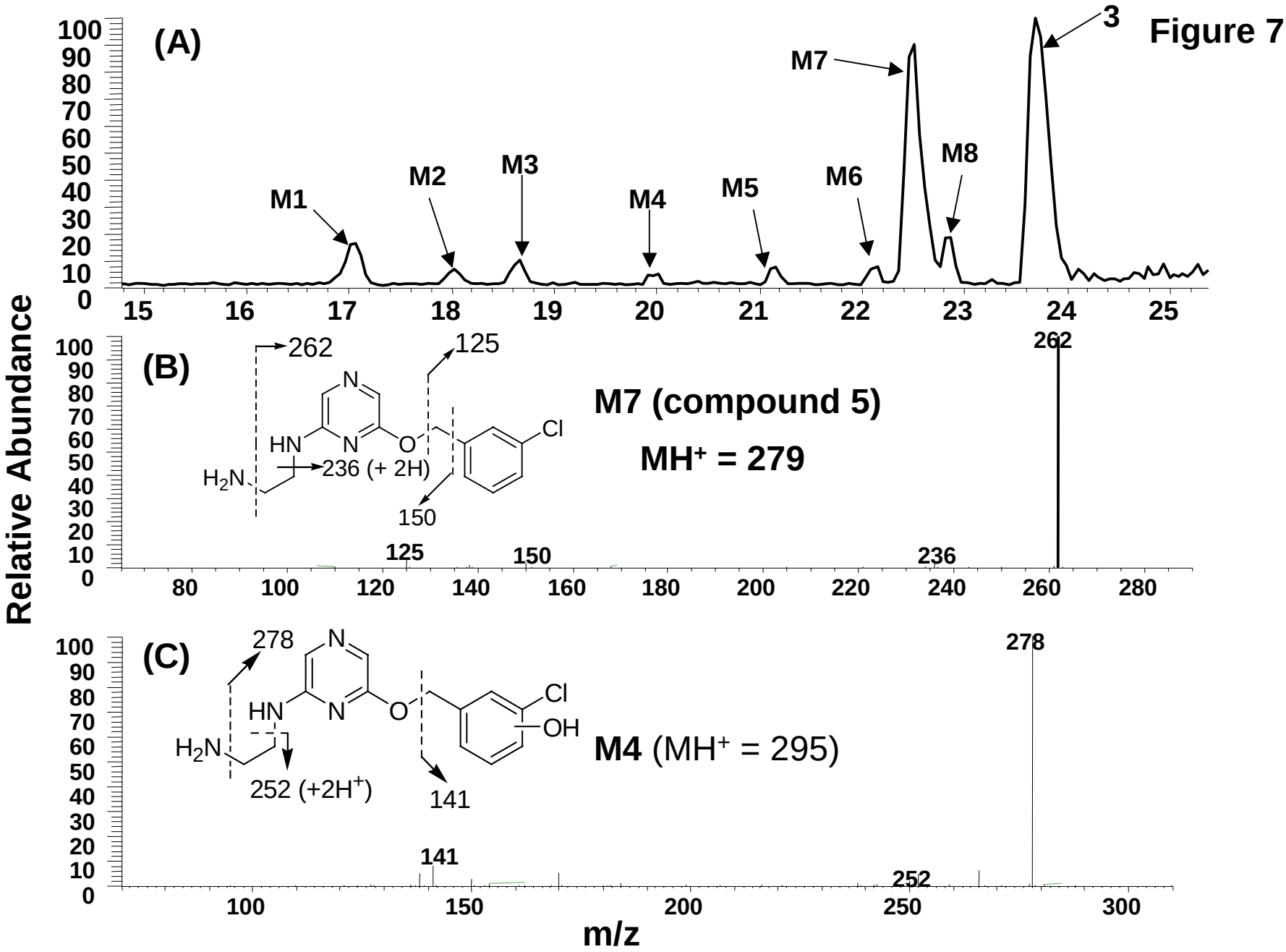

DMD Fast Forward. Published on March 7, 2007 as DOI: 10.1124/dmd.106.013649
This article has not been copyedited and formatted. The final version may differ from this version.

Downloaded from dmd.aspetjournals.org at ASPET Journals on May 23, 2024

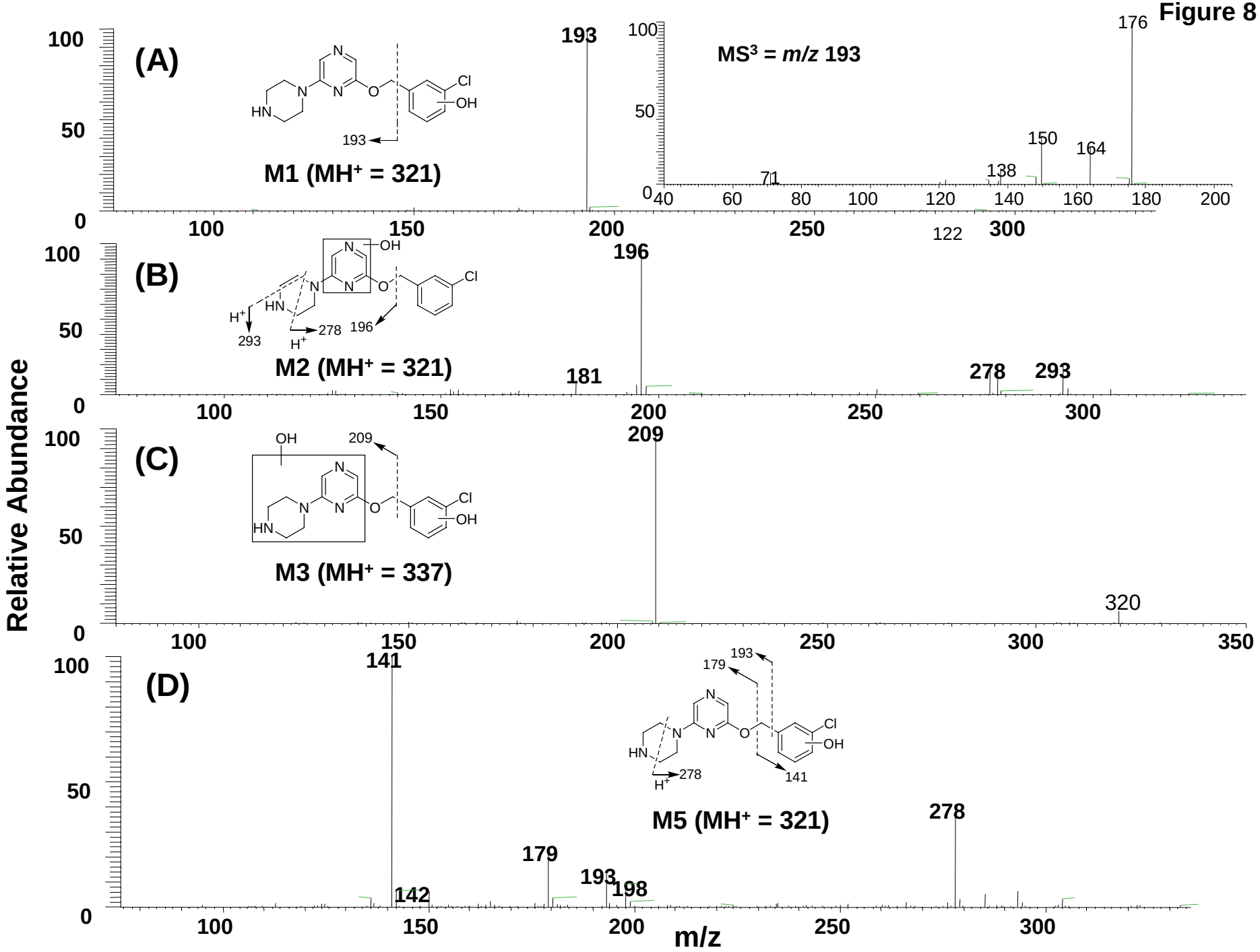

DMD Fast Forward. Published on March 7, 2007 as DOI: 10.1124/dmd.106.013649
This article has not been copyedited and formatted. The final version may differ from this version.

Downloaded from dmd.aspetjournals.org at ASPET Journals on May 23, 2024

Figure 9

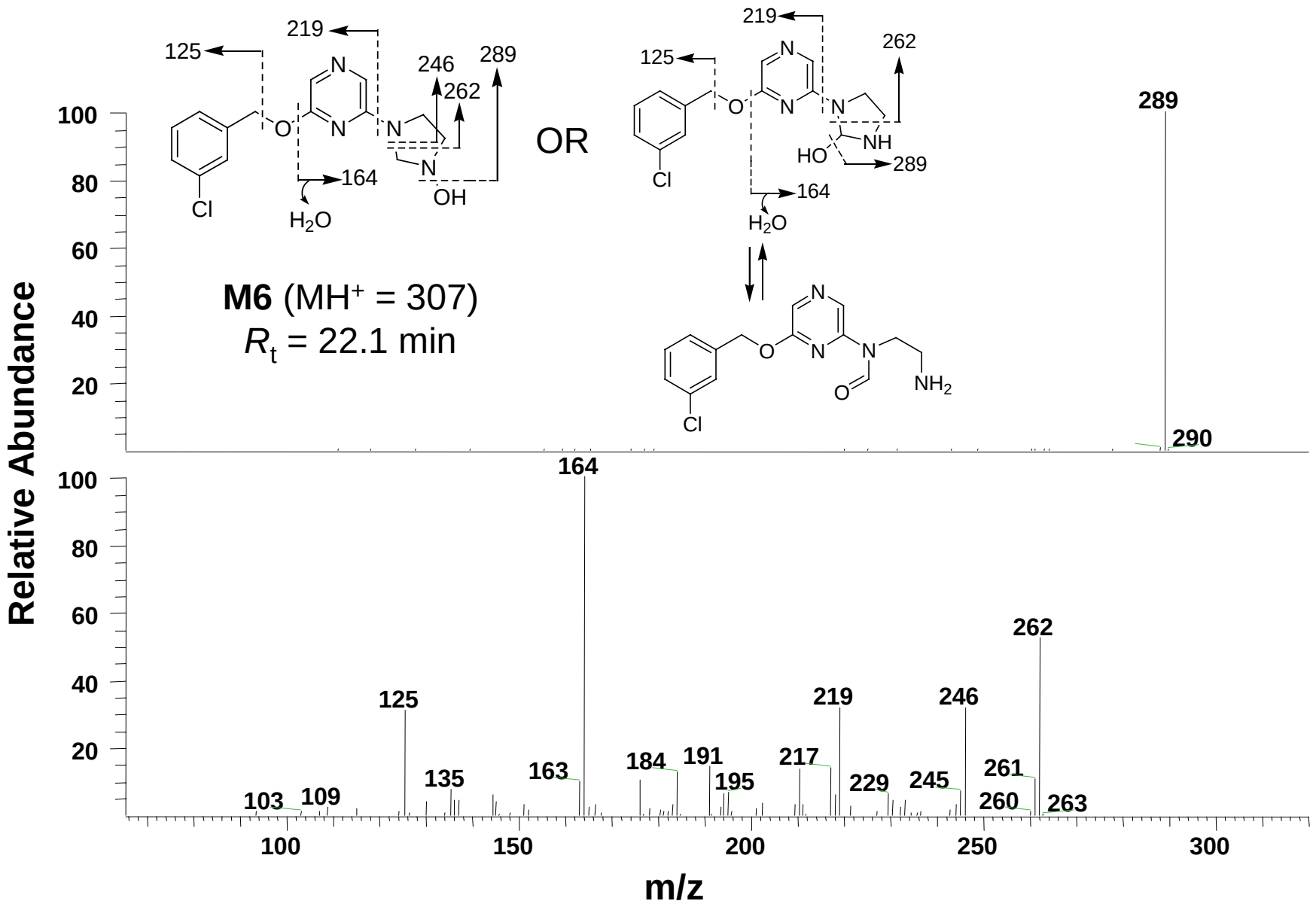

DMD Fast Forward. Published on March 7, 2007 as DOI: 10.1124/dmd.106.013649
This article has not been copyedited and formatted. The final version may differ from this version.

Downloaded from dmd.aspetjournals.org at ASPET Journals on May 23, 2024

Figure 10

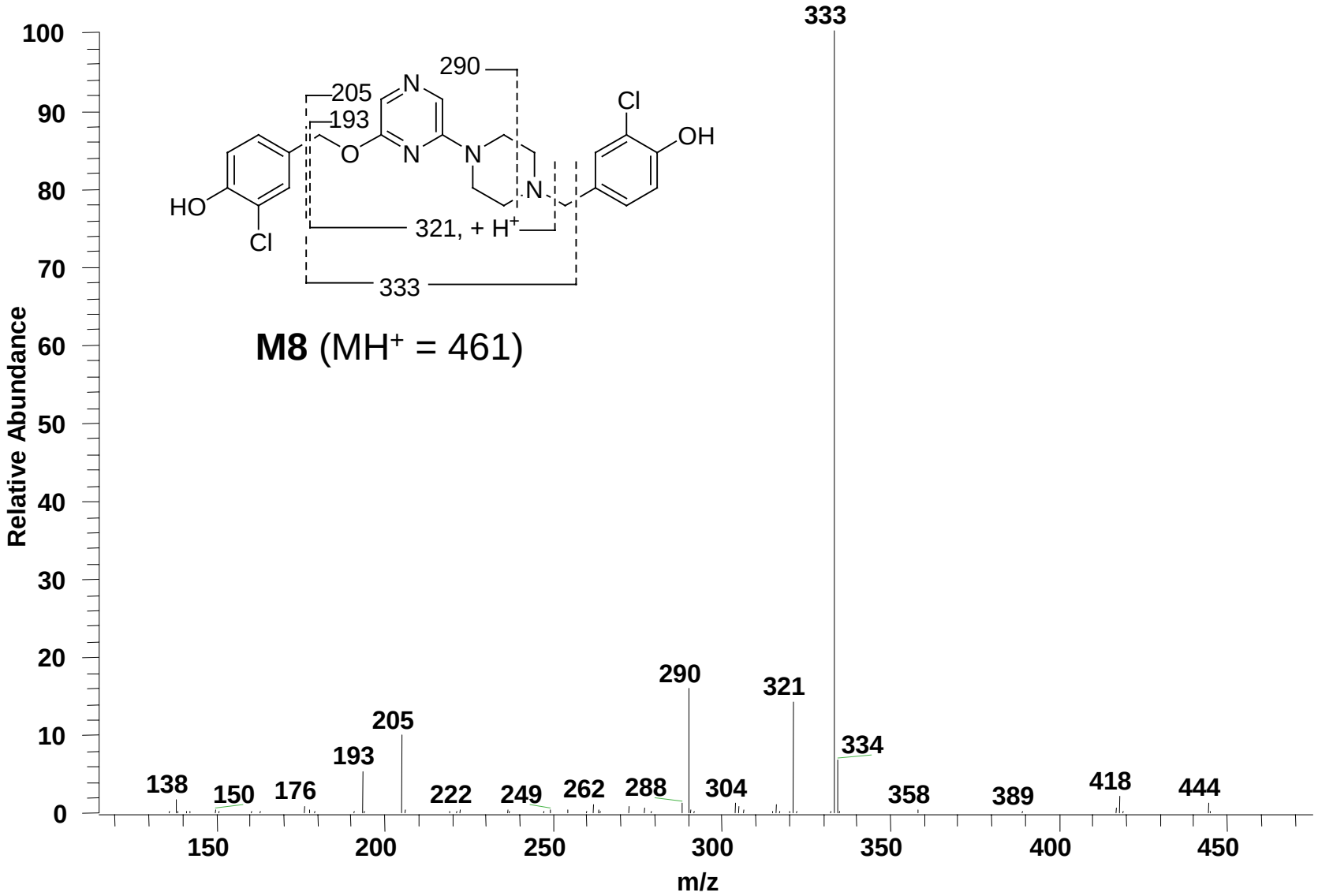

DMD Fast Forward. Published on March 7, 2007 as DOI: 10.1124/dmd.106.013649
This article has not been copyedited and formatted. The final version may differ from this version.

Downloaded from dmd.aspetjournals.org at ASPET Journals on May 23, 2024

Figure 11

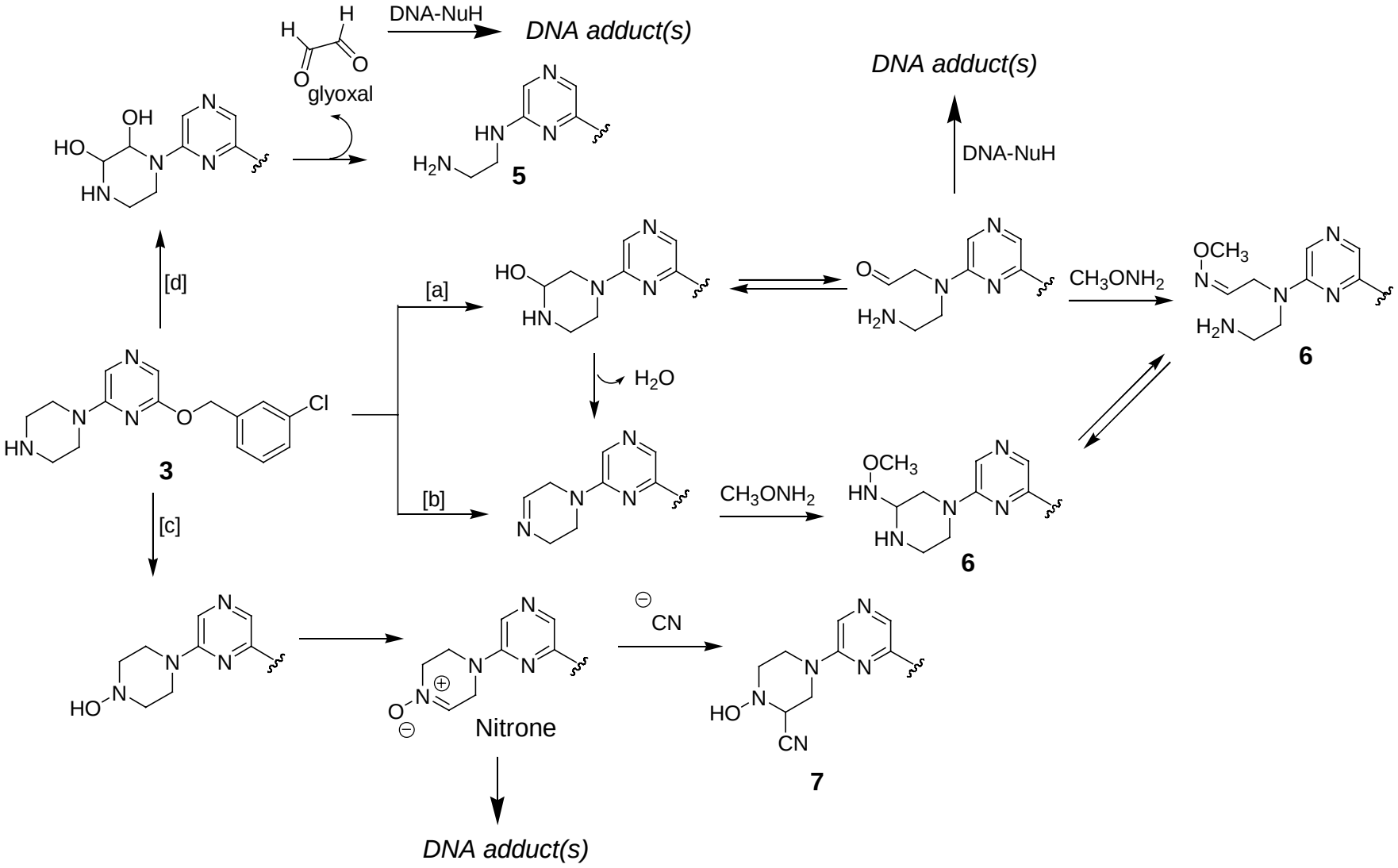

DMD Fast Forward. Published on March 7, 2007 as DOI: 10.1124/dmd.106.013649
This article has not been copyedited and formatted. The final version may differ from this version.

Downloaded from dmd.aspetjournals.org at ASPET Journals on May 23, 2024

Figure 12

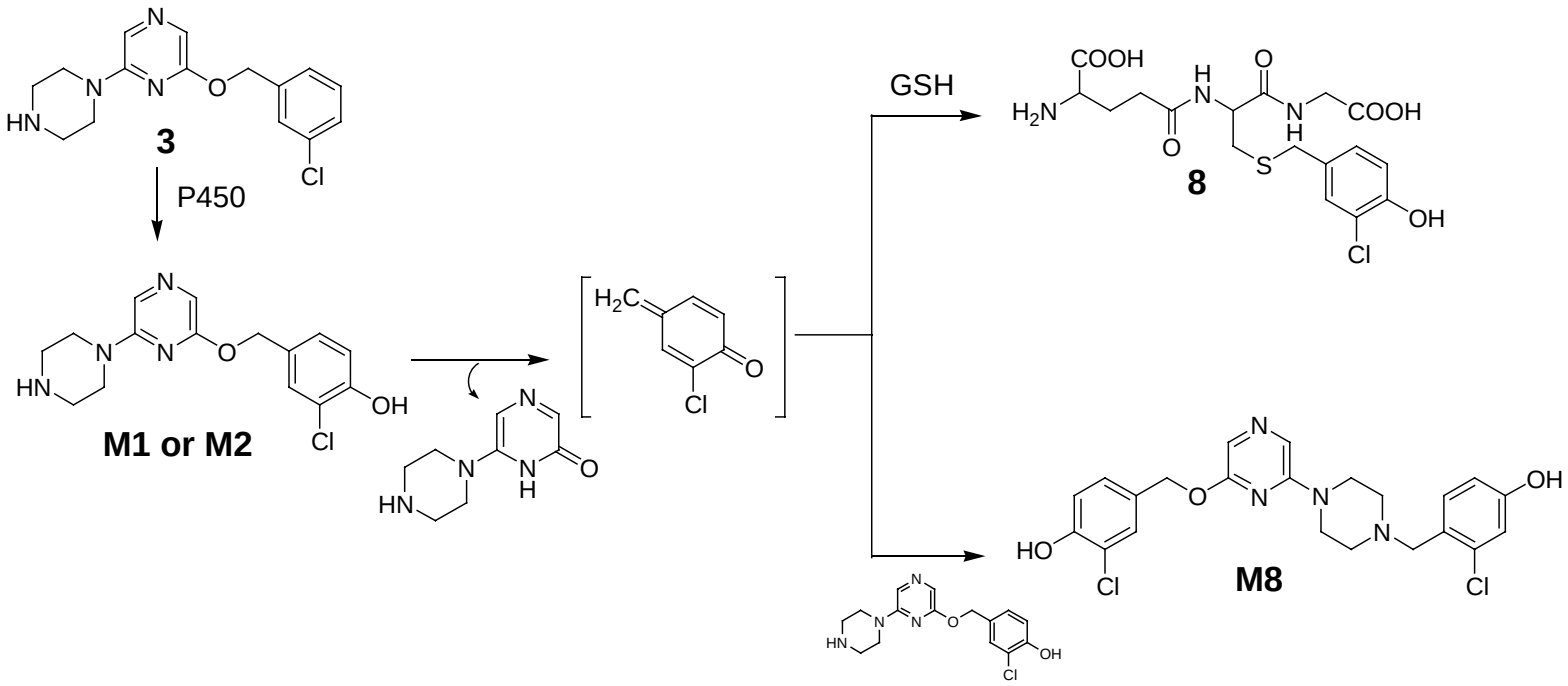

DMD Fast Forward. Published on March 7, 2007 as DOI: 10.1124/dmd.106.013649
This article has not been copyedited and formatted. The final version may differ from this version.

Downloaded from dmd.aspetjournals.org at ASPET Journals on May 23, 2024